Theses and Dissertations                                      1. Thesis and Dissertation Collection, all items

2007-12

# Multiscale modeling of flows containing particles

Alrowaijeh, Jamal S.

Monterey California. Naval Postgraduate School

http://hdl.handle.net/10945/3082

# NAVAL POSTGRADUATE SCHOOL

## MONTEREY, CALIFORNIA

# THESIS

**MULTISCALE MODELING OF FLOWS CONTAINING PARTICLES**

by

Jamal Salem AlRowaijeh

December 2007

Thesis Advisor:                                   Young W. Kwon

**Approved for public release; distribution is unlimited**

THIS PAGE INTENTIONALLY LEFT BLANK

| REPORT DOCUMENTATION PAGE | | *Form Approved OMB No. 0704-0188* |
|---|---|---|
| Public reporting burden for this collection of information is estimated to average 1 hour per response, including the time for reviewing instruction, searching existing data sources, gathering and maintaining the data needed, and completing and reviewing the collection of information. Send comments regarding this burden estimate or any other aspect of this collection of information, including suggestions for reducing this burden, to Washington headquarters Services, Directorate for Information Operations and Reports, 1215 Jefferson Davis Highway, Suite 1204, Arlington, VA 22202-4302, and to the Office of Management and Budget, Paperwork Reduction Project (0704-0188) Washington DC 20503. | | |
| **1. AGENCY USE ONLY** *(Leave blank)* | **2. REPORT DATE**<br>December 2007 | **3. REPORT TYPE AND DATES COVERED**<br>Master's Thesis |
| **4. TITLE AND SUBTITLE** Multiscale Modeling of Flows Containing Particles | | **5. FUNDING NUMBERS** |
| **6. AUTHOR(S)** Jamal S. AlRowaijeh | | |
| **7. PERFORMING ORGANIZATION NAME(S) AND ADDRESS(ES)**<br>Naval Postgraduate School<br>Monterey, CA 93943-5000 | | **8. PERFORMING ORGANIZATION REPORT NUMBER** |
| **9. SPONSORING /MONITORING AGENCY NAME(S) AND ADDRESS(ES)**<br>N/A | | **10. SPONSORING/MONITORING AGENCY REPORT NUMBER** |
| **11. SUPPLEMENTARY NOTES** The views expressed in this thesis are those of the author and do not reflect the official policy or position of the Department of Defense or the U.S. Government. | | |
| **12a. DISTRIBUTION / AVAILABILITY STATEMENT**<br>Approved for public release; distribution is unlimited | | **12b. DISTRIBUTION CODE** |

**13. ABSTRACT (maximum 200 words)**

Multiscale mathematical modeling of flows containing particles is conducted in this study using computational fluid dynamics and molecular dynamics. The first study considered continuous media interaction of macro-scale fluid and micro-scale solid particles using computational fluid dynamics and rigid particle dynamics. This study investigates the potential enhancement of heat transfer properties of particulate fluid as well as the effect of injected particles on fluid profiles, and pressure on walls under different particle injection conditions. In the second part of this research, the molecular dynamics simulation was performed to simulate solid-liquid interaction at the molecular level (nanotechnology) to understand their behaviors. The results from two different scales were compared qualitatively.

| **14. SUBJECT TERMS** Multiscale Mathematical Modeling, Particle-Fluid Interaction, Continuum Model, Atomic Model | | | **15. NUMBER OF PAGES**<br>95 |
|---|---|---|---|
| | | | **16. PRICE CODE** |
| **17. SECURITY CLASSIFICATION OF REPORT**<br>Unclassified | **18. SECURITY CLASSIFICATION OF THIS PAGE**<br>Unclassified | **19. SECURITY CLASSIFICATION OF ABSTRACT**<br>Unclassified | **20. LIMITATION OF ABSTRACT**<br>UU |

NSN 7540-01-280-5500

Standard Form 298 (Rev. 2-89)
Prescribed by ANSI Std. 239-18

THIS PAGE INTENTIONALLY LEFT BLANK

**MULTISCALE MODELING OF FLOWS CONTAINING PARTICLES**

Jamal S. AlRowaijeh
Lieutenant Commander, Royal Bahraini Naval Force
B.S., Military Technical College, Cairo, 1993

Submitted in partial fulfillment of the
requirements for the degree of

**MASTER OF SCIENCE IN MECHANICAL ENGINEERING**

from the

**NAVAL POSTGRADUATE SCHOOL**
**December 2007**

Author:          Jamal S. AlRowaijeh

Approved by:     Young W. Kwon
                 Thesis Advisor

                 Anthony J. Healey
                 Chairman, Department of Mechanical Engineering and Astronautic
                 Engineering

THIS PAGE INTENTIONALLY LEFT BLANK

# ABSTRACT

Multiscale mathematical modeling of flows containing particles is conducted in this study using computational fluid dynamics and molecular dynamics. The first study considered continuous media interaction of macro-scale fluid and micro-scale solid particles using computational fluid dynamics and rigid particle dynamics. This study investigates the potential enhancement of heat transfer properties of particulate fluid as well as the effect of injected particles on fluid profiles, and pressure on walls under different particle injection conditions. In the second part of this research, the molecular dynamics simulation was performed to simulate solid-liquid interaction at the molecular level (nanotechnology) to understand their behaviors. The results from two different scales were compared qualitatively.

THIS PAGE INTENTIONALLY LEFT BLANK

# TABLE OF CONTENTS

# LIST OF FIGURES

x

# LIST OF TABLES

THIS PAGE INTENTIONALLY LEFT BLANK

# ACKNOWLEDGMENTS

I would like to express my greatest thanks to my advisor, Professor Young W. Kwon, for the great effort that he has made throughout my long research activities. His influence in teaching me the fundamentals of solid mechanics as well as the finite element method and molecular dynamics techniques has encouraged me to pursue this field of interest in my current and future study and research.

Also, I would like to thank Professor Garth Hobson for his continuous extensive support in teaching me different finite element method programs and computational fluid dynamics commercial programs. I will not forget the high level of professionalism shown by members of mechanical engineering department at the Naval Postgraduate School. To them I address my best thanks.

Finally, I would like to thank my parents, wife and my children Duaa, Salem, Hamad and Arwa for their great support and patience during my study in Monterey at NPS.

THIS PAGE INTENTIONALLY LEFT BLANK

# I.     INTRODUCTION

## A.     BACKGROUND

Solid-liquid interactions problems can be found in many current multi-physics civil and military applications. These applications include, but are not limited to, bridges, flow passing over cylinders, underwater weapons, internal combustion engines, civil structures, and solid particles injection. Due to the complexity of these types of coupled problems, numerical techniques such as Finite Element Method(FEM) and Computational Fluid Dynamics(CFD) were developed and used in many multi-physics problems to obtain accurate simulation results for the required application in order to avoid any unexpected failure in real future applications, and to improve the performance of the systems [1], [2].

The micro-and nano world is a very tiny and complicated world to analyze. In order to be able to study the nature and the behavior of the micro-and nano-world, we need accurate, sensitive and expensive measurement devices to observe the multiphase interaction on an atomic scale. However, the recent development of current commercial programs provides accurate simulation results for different kinds of tiny multi-scale applications without the need to use such expensive and advanced measurement instruments [2].

For current advances in nanotechnology applications, micro/nano solid particles injection becomes an important research field in the coupled dynamical interaction between solid phase and liquid phase applications. Research interest in this field has seen great growth in recent years, especially in the medical and chemical fields [2], [3].

The solid particles phase and fluid phase will exchange momentum and the nature, characteristics of  the particles physical properties and its motion will control the amount of fluid-solid phases heat and mass transfer (HMT) that are associated with the chemical reactions [2], [3]. Heat and mass transfer are very important factors in computational mechanics and multiphase applications, and therefore many commercial

programs were developed to track the particles' trajectory through the computational domain. The analysis of the movement and the trajectory of the particles in the computational domain containing a fluid can be performed by using FEM and solving the equations of the mass, momentum and energy conservation for both the solid and liquid in a Lagrangian frame of reference which is known as a Lagrangian description/formulation. In the most advanced current simulation programs the solid particles' discrete phase can exchange mass, drag, and heat energy with the surrounding ambient fluid continuous phase [1], [3], [4], [5].

CFD simulation programs have many limitations including the size of the injected particles and the assumed particles' constant viscosity during the simulation process, which is not always true in many internal combustion engines applications. The alternative solution is using the Molecular Dynamic Simulation (MDS) to analyze some of the critical engineering applications [6].

Molecular Dynamic Simulation (MDS) is performed to calculate the mechanical properties of interest, such as thermal conductivity, for a nano-scale model. Molecular dynamic (MD) is a very simple and powerful simulation technique that can be used for solving the equation of motion of a system of molecules without any limitations [6], [7]. In molecular dynamics all the calculations performed are physically based, and can be performed without the need for any assumptions. All the calculations are based on the Lennard-Jones (L.J) 6-12 intermolecular potential. Then, thermodynamics and other mechanical properties can be calculated without any assumptions [6].

Furthermore, transport of the atomic particles through the simulation model can be used to calculate the thermal conductivity and any other physical properties of interest that can be obtained from the intermolecular potential of the system of molecules of interest [7]. In our research, this technique is performed to study the behavior of the interacted atoms in the simulation domain under different solid-liquid particles' molecular interaction.

## B.	OBJECTIVES

The present studies conducted multiscale mathematical modeling of flows containing particles using computational fluid dynamics and molecular dynamics. The first study considered continuous media interaction of macro-scale fluid and micro-scale solid particles using computational fluid dynamics and rigid particle dynamics. The objectives of this study were to investigate the potential enhancement of heat transfer properties of particulate fluids as well as the effect of injected particles on fluid profiles, and the pressure on walls under different particle injection conditions.  In the second part of this research, the molecular dynamics simulation was performed to simulate solid-liquid interaction at the molecular level (nanotechnology) to understand their behaviors.

## C.	LITERATURE SURVEY

There is an extensive amount of literature available for Solid-Liquid Interaction (SLI). However, some of the papers that contain particles injection and molecular dynamic simulations are represented here to introduce both simulation techniques.

Most of the work done in the past concentrated on injection into internal combustion engines such as the petrol engine, diesel engines and gas turbine engines. Work was concentrated into two fields of interest: an investigation into flow properties around injected fuel particles, such as solving the equation of motion of momentum and energy near the fuel droplet [3].

The second field concentrated on investigating the transport particles associated with a change in phase by using two different models. The first was the trajectory model while the second was the effective-continuum model [3].

Many numerical solution methods were developed in order to achieve the objectives of particles flow. These methods were applied to the heat and mass transfer around the transport particles [3].

For the multiphase coupled problems, SLI is one important application. Some of the current simulations used the particle finite element technique. The technique depends on the use of the Lagrangian equations to simulate the transport of the particles in the fluid-structure calculation domain in which the particles are represented by the nodes [4].

The current simulation program used for the fluid phase is the Navier-Stokes based simulation, without any restriction on the fluid properties. [8]. For steady state calculations, the injected transport particles are tracked until they leave the domain or are otherwise specified by the user by solving the Lagrange's equation. Each particle tracked by the CFD ACE code represents the behavior of a large number of conglomerated particles [1].

Recent molecular dynamic simulation programs are widely used and developed. There are many papers in this field of study, especially for physics, material science, and combustion applications [6], [9]. The molecular dynamic technique can be used to solve current coupled flow problems that can be found in many solid liquid interaction applications. All transport physical properties such as viscosity and thermal conductivities come from the intermolecular force [12-6] (Lennard-Jones potential) between the particles. All other positions, velocities, and accelerations of the atoms can be calculated from the L-J potential. The MD simulation accuracy depends on two important factors: the intermolecular potential and the finite difference scheme [6].

Another significant paper discussed a new method for the coupling continuum molecular-dynamics simulation. This method used a 3-D micro channel system of molecules to simulate the flow of liquids where the atoms interacted with each other based on (L-J) [12-6] potential, and periodic boundary conditions were applied. [10]. Also, since the first two units of the wall atoms were constrained, this simulation depends on using different energy values such that $\varepsilon_{ww} = 5\varepsilon_{wl} = 5\varepsilon_{ll}$ for the wall and liquid, Furthermore, different values of masses for the solid and liquid atoms were used $\left( m_w = 5m_l \right)$ [10].

# II.    MODELING, MACRO-SCALE MODEL

Recently, many commercial programs have demonstrated successful development in simulating different kinds of engineering problems such as solid particles injection. The particles injection technology is widely used in different engineering applications, such as

1.      Fuel combustion in internal combustion engines (ICE).

2.      Thermal spray in advanced coating applications.

3.      Rooms applications such as dust movement.

In addition, there are many other heat transfer, medical and other biological defense applications [4].

Most of the current engineering problems have many engineering aspects interacting together. Therefore, the simulation of these types of coupled problems must be performed by using multi-physics capable commercial programs like FLUENT, ANSYS, COMSOL and CFD+ACE. In this research, we used the software package provided by CFD+ACE because of its ability to simulate these kinds of engineering problems that contain particles injection/spray. Many programs' modules were used during the simulation of particles injection; these modules are listed below.

## A.      SPRAY MODULE

For the steady state calculations, the tracking of the injected/sprayed particles can be analyzed by solving the Lagrangian formulation. The particle tracking through the calculation domain can be performed until it leaves the domain or to a point otherwise specified by the user. Furthermore, the behavior of the injected particles can be obtained by tracking a single particle [4].

The particle equation of motion is given by

$$m_p \frac{\partial v}{\partial t} = C_d \cdot \rho \cdot (U - v) \cdot |U - v| \cdot \frac{A_p}{2} + m_p \cdot g \qquad (2.1)$$

where $m_p$ is the injected particle mass, $v$ is the particle velocity vector expressed as $v = (u_i + v_j + w_k)$, and $C_d$ is the coefficient of the drag and is a function of the Reynolds number, which can be written as

$$R_e = \frac{\rho \cdot |U - v| \cdot d}{\mu}. \qquad (2.2)$$

$A_p$ is the frontal area of the particle, and for spherical particles it can be written as

$$A_p = \frac{\pi \cdot r^2}{16} \qquad (2.3)$$

in which $r$ is the particle's radius, $\rho$ is the surrounding fluid density , $U$ is the ambient fluid velocity, $p$ is the surrounding fluid pressure, and $g$ is the gravity.

In this research, the working fluid used is water and for the incompressible flow, the drag coefficient is given by

$$C_d = \frac{24}{R_e} \qquad \text{for } R_e < 1$$

$$C_d = \frac{24}{R_e} \left[ 1 + 0.15 R_e^{0.687} \right] \qquad \text{for } 1 < R_e < 10^3 \qquad (2.4)$$

$$C_d = 0.44 \qquad \text{for } R_e > 10^3$$

## 1. Limitations of the Spray/Injection

Some limitations and assumptions of the CFD ACE spray module are stated below: [4]

(1)     The displaced volume of the particles caused by its transport motion through the computational domain are neglected.

6

(2)     The particle internal temperature change during the simulation process is neglected.

(3)     The simulated injected/sprayed particle is represented in CFD ACE+ multipysics solver by a single part.

### 2.     Spray Module Grid Limitations

The size of the grid cell of the computational domain must be generated such that its size is much larger than the particle/droplet size to ensure obtaining accurate simulation results. Furthermore, in order to ensure an accurate result for these types of problems, the 4th order magnitude of convergence is required here, and this can be obtained by the methodology explained in the CFD+ACE modules manual [1].

### 3.     Spray Wall Boundary Treatment

In the current simulation, the injected particles are not allowed to bounce or reflect after hitting the wall. Instead, they vanish, and the program will stop tracking it as soon as particles hit the wall. In some of our preliminary analysis, one example of bounced particle is introduced only to show the effect of particles injection on pipe/tube clogging.

## B.     FLUID MODULE

The liquid simulation used in the program solves the Navier-Stokes equations. The momentum equation can written as

$$\frac{\partial u}{\partial t} = -(u \cdot \nabla)u - \frac{1}{\rho}\nabla \cdot p + v \cdot \nabla^2 \cdot u + \mathbb{F},$$     (2.5)

and for incompressible flow

$$\nabla \cdot u = 0$$     (2.6)

where the liquid properties $\rho$ is the fluid density, $v$ is the liquid viscosity, $p$ is the liquid pressure, and $\mathbb{F}$ is the applied external force [8].

## C.    HEAT TRANSFER MODULE

The heat transfer module numerically solves for the energy (total enthalpy) equation in the system [1]. The conservation of energy equation can be written as

$$\frac{\partial(\rho \cdot h_0)}{\partial t} + \nabla \cdot (\rho \cdot \vec{V} \cdot h_0) =$$

$$\nabla \cdot (k_{eff} \cdot \nabla \cdot T) + \frac{\partial p}{\partial t} + \left[ \frac{\partial(u\tau_{xx})}{\partial x} + \frac{\partial(u\tau_{yx})}{\partial y} + \frac{\partial(u\tau_{zx})}{\partial z} \right]$$

$$+ \left[ \frac{\partial(u\tau_{xy})}{\partial x} + \frac{\partial(u\tau_{yy})}{\partial y} + \frac{\partial(u\tau_{zy})}{\partial z} \right] + \left[ \frac{\partial(u\tau_{xz})}{\partial x} + \frac{\partial(u\tau_{yz})}{\partial y} + \frac{\partial(u\tau_{zz})}{\partial z} \right] + S_h \qquad (2.7)$$

where $h_0$ is the total enthalpy and is given by

$$h_0 = e + \frac{p}{\rho} + \frac{1}{2} \cdot (u^2 + v^2 + w^2) \qquad (2.8)$$

in which $e$ is the internal energy, $p$ is the pressure, $\tau_{ij}$ is the stress tensor and $k_{effective}$ is the material effective thermal conductivity. In laminar flow it is the thermal conductivity of the fluid, and in the turbulent flow it is given by

$$k_{effective} = K + \frac{u_t C_p}{\sigma_t} \qquad (2.9)$$

in which $\sigma_t$ is the turbulent Prandtl number and $S_{heat}$ is additional heat sources term.

The heat source term of equation [1.7] for the spray is given by

$$S_{heat} = 1 + \frac{1}{3} \cdot R_e^{(1/2)} \cdot N_{sc}^{(1/3)} \qquad (2.10)$$

in which the term $N_{sc}$ represents the Schmidt number.

## D. TURBULENCE MODULE

The $k - \varepsilon$ model used in the CFD + ACE turbulence module is based on solving equations of motion of the turbulence kinetic energy and the rate of dissipation $k$ and $\varepsilon$ respectively [1].

The equations of motion are given by

$$\frac{\partial}{\partial t}(\rho \cdot k) + \frac{\partial}{\partial x_j}(\rho \cdot u_j \cdot k) = \rho \cdot p - \rho \cdot \varepsilon + \frac{\partial}{\partial x_j}\left[\left(\mu + \frac{\mu_t}{\sigma_k}\right)\frac{\partial k}{\partial x_j}\right] \tag{2.11}$$

$$\frac{\partial}{\partial t}(\rho \cdot \varepsilon) + \frac{\partial}{\partial x_j}(\rho \cdot u_j \cdot \varepsilon) = C_{\varepsilon_1}\frac{\rho \cdot p \cdot \varepsilon^2}{k} - C_{\varepsilon_2}\frac{\rho \cdot \varepsilon^2}{k} + \frac{\partial}{\partial x_j}\left[\left(\mu + \frac{\mu_t}{\sigma_\varepsilon}\right)\frac{\partial \varepsilon}{\partial x_j}\right] \tag{2.12}$$

where $p$ is the production term and can be written as

$$p = v_t\left(\frac{\partial u_i}{\partial x_j} + \frac{\partial u_j}{\partial x_i} - \frac{2}{3}\frac{\partial u_m}{\partial x_m}\delta_{ij}\right)\frac{\partial u_i}{\partial x_j} - \frac{2}{3}k\frac{\partial u_m}{\partial x_m} \quad . \tag{2.13}$$

The viscosity of the turbulence can be written as

$$\gamma_t = \frac{C_\mu \cdot k^2}{\varepsilon} \quad . \tag{2.14}$$

The constants of equations (2.11) and (2.12) are given by

$$C_\mu = 0.09, C_{\varepsilon_1} = 1.44, C_{\varepsilon_2} = 1.92, \sigma_k = 1.0 \text{ and } \sigma_\varepsilon = 1.3 .$$

THIS PAGE INTENTIONALLY LEFT BLANK

# III.    NANO-SCALE MODEL, MD SIMULATION

## A.    MOLECULAR DYNAMIC, THE TECHNIQUE

Molecular dynamics simulations can be used to model current complicated multiphase applications. Due to the simplicity of this program, there is no need to consider any kind of assumptions. The physical properties can be obtained from the force that results from the (L-J) [12-6] intermolecular potential. Then the physical properties of interest can be evaluated from a program such as thermal conductivity [6], [12].

Molecular dynamics has many advantages in solving critical applications, such as the combustion in internal combustion engines. Unlike the other commercial computational fluid mechanics programs, molecular dynamics doesn't require many assumptions; e.g., the CFD programs has many limitations in the shape of the droplet/particle, and it considers a constant viscosity for the simulated fluid during the whole simulation process [6], [12].

Nowadays, molecular dynamics as a powerful technique is used in many applications, including but not limited to chemistry and material science [13], [14].  In this research the MD simulation was conducted to study the behavior of the interacted atoms in a system of molecules, and to study the effect of the particles on the flow of the fluid atoms under different simulation conditions. Molecular dynamics program calculations depend on two important factors: the intermolecular potential and the finite difference method [6].

For molecular dynamics, the program was written in FORTRAN language code, and it contains three main simulation processes. These processes are initialization, equilibrium, and production [17].

## 1. Potential

As stated above, the molecular dynamics simulation depends on solving the Lennard-Jones intermolecular potential. The (L-J) intermolecular potential for soft sphere can be written as [15], [16]

$$u(r) = k\varepsilon \left[ \left( \frac{\sigma}{r} \right)^n - \left( \frac{\sigma}{r} \right)^m \right] \tag{3.1}$$

in which

$$k = \frac{n}{n-m} \left( \frac{n}{m} \right)^{m/(n-m)} . \tag{3.2}$$

The widely used values of the terms $n$ and $m$ are $n = 2m$, where $n = 6$ [17]. The Lennard-Jones interaction potential can be written as

$$u(r) = 4\varepsilon \left[ \left( \frac{\sigma}{r} \right)^6 - \left( \frac{\sigma}{r} \right)^{12} \right] \tag{3.3}$$

where $\sigma$ and $\varepsilon$ are the distance to zero and the energy at the minimum in the Lennard-Jones potential function as indicated in Figure 1. Figure 1 shows the Lennard-Jones [12-6] potential in which $u^* = u / \varepsilon$ and $r^*$ is the distance between atom and it is given by $r^* = r / \sigma$ [17].
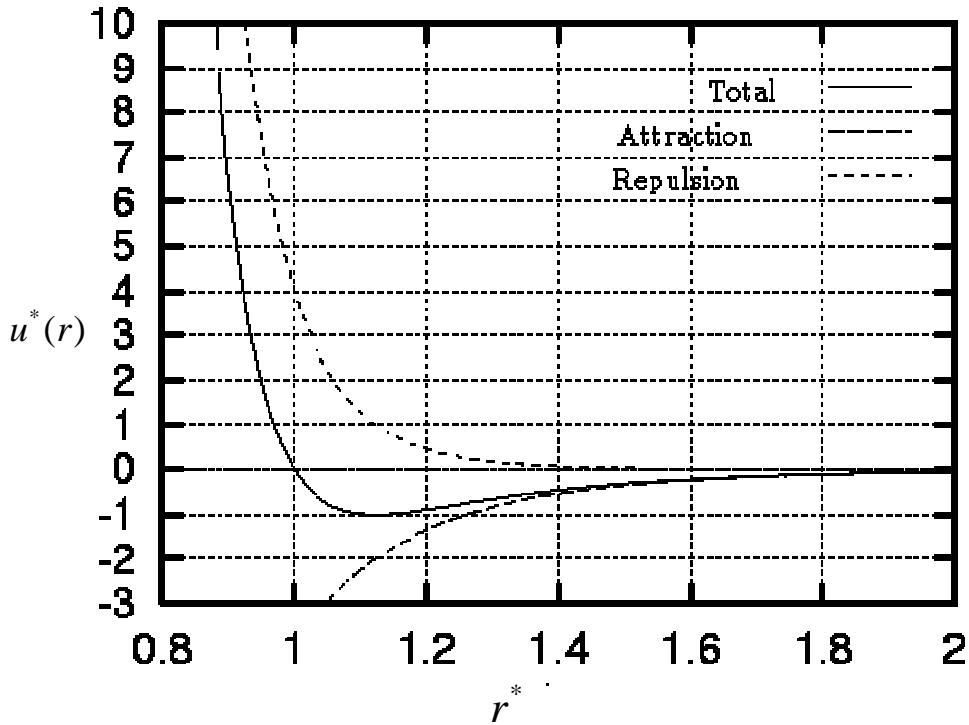
Figure 1.　　Lennard-Jones [12-6] Potential (from [18])

The intermolecular force that results from the potential can be obtained by taking the derivatives of Equation (3.2) with respect to the atomic distance. The intermolecular force is given by

$$F(r) = \frac{-du(r)}{dr} = \frac{24\varepsilon}{\sigma}\left[2\left(\frac{\sigma}{r}\right)^{13} - \left(\frac{\sigma}{r}\right)^{7}\right].$$

(3.4)

Molecular dynamics program requires long computational time [6], and therefore to reduce the simulation time, we can neglect the calculations at certain critical atomic distance $r_{critical}$ [17]. The Lennard-Jones potential becomes

$$u(r) = \begin{cases} 4\varepsilon\left[\left(\frac{\sigma}{r}\right)^{12} - \left(\frac{\sigma}{r}\right)^{6}\right] & r \leq r_{critical} \\ 0 & r \geq r_{critica} \end{cases}$$

(3.5)

13

## 2. Finite Difference Method

The finite difference method plays an important role in the molecular dynamic simulation. Newton's second law of motion is given by

$$F_i = ma_i \tag{3.6}$$

where $F_i$ is the intermolecular force, $m$ is the atom mass, and $a_i$ is the atom acceleration. In this research, the Verlet finite difference scheme was used to compute new velocities and positions from the acceleration vectors [6], [17]. The Verlet finite difference scheme is given by the following equations

$$v\left(t + \frac{\Delta t}{2}\right) = v\left(t - \frac{\Delta t}{2}\right) + a(t)\Delta t \tag{3.7}$$

$$r\left(t + \Delta t\right) = \Delta t v\left(t + \frac{\Delta t}{2}\right) + r(t) \tag{3.8}$$

$$v(t) = \frac{v}{2}\left(t + \frac{\Delta t}{2}\right) + \frac{v}{2}\left(t - \frac{\Delta t}{2}\right). \tag{3.9}$$

There are many advantages of using the Verlet scheme, such as simulation stability and calculations simplicity [17].

## B. PROPERTIES CALCULATIONS

Many physical (static and dynamic) properties can be obtained, as stated before, from the Lennard-Jones intermolecular potential between the atoms. The static properties include thermodynamic properties such as internal energy, temperature, and pressure and the dynamic properties like shear viscosity [6], [17].

## C.    MOLCULAR DYNAMICS SIMULATION

In this research, the molecular dynamic program was used to simulate multiphase solid-liquid interaction flow under different particle locations in order to observe the behavior of atoms in the domain.

### 1.    Simulation Formulation

The 3-D micro-channel used in the current simulation is represented by a lattice atomic configuration such that the number of atomic units in $x-direction = 10$ units, $y-direction = 1$ unit, and $z-direction = 20$ units; this resulted in 800 atoms. The first upper and lower atoms line of the computational domain are constrained to simulate the fluid flow through the nano-channel, and then the attached two atomic units to the first atoms are considered as solid atoms.

After that, the remaining atoms located between the solid atoms are considered as liquid atoms. The wall, solid, and liquid atoms masses are assigned in the following way: $m_w = m_s = 3m_l$ respectively. The distance to zero $\sigma$ were assigned an equal value of $\sigma = 2$ while the energy at the minimum $\varepsilon$ were assigned in the following way: $\varepsilon_w = 0.5$, $\varepsilon_s = 0.5$, and $\varepsilon_f = 0.1$ for the wall, solid, and liquid atoms, respectively, while the energy value between the wall, solid, and liquid atoms were assigned the following values: $\varepsilon_{ws} = 0.5$, $\varepsilon_{wl} = 0.2$, and $\varepsilon_{sl} = 0.2$.

The result of running the simulation for 10,000 iterations with $x-direction$ velocity $f_x = 0.1$ is shown in Figure 2. This figure shows the resulted atoms configuration (red) compared to the original configuration (blue) atoms. From the figure it is clear that the fluid atoms have a higher amount of vibration compared to that in solid atoms.

15
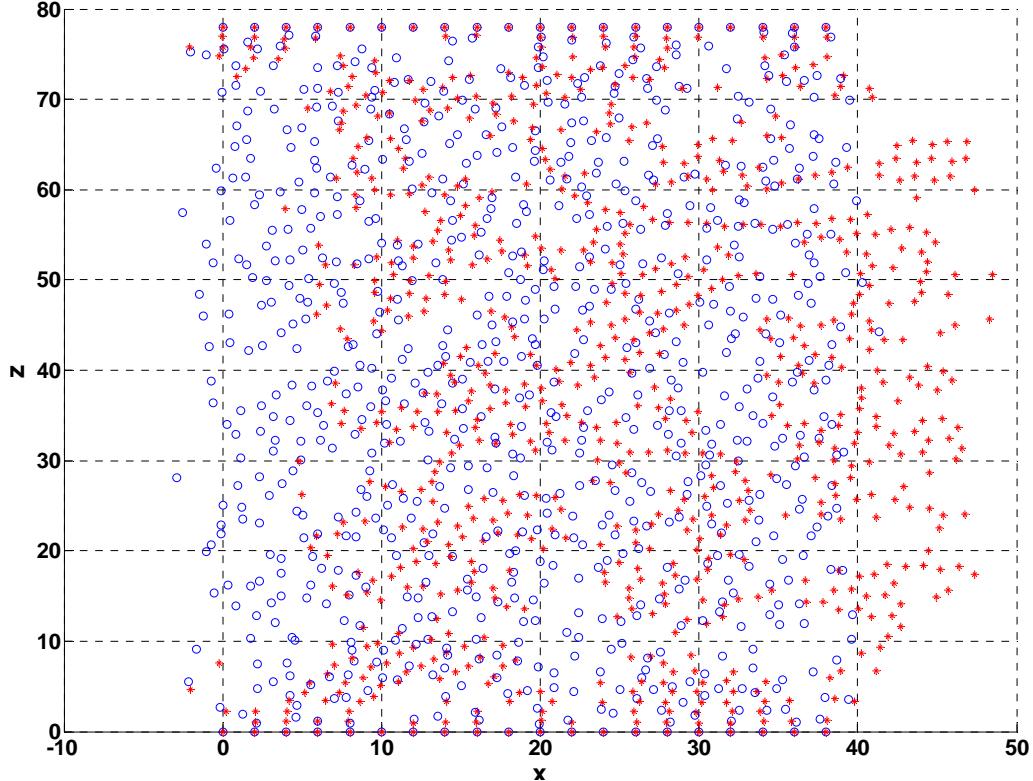
Figure 2.        Original and final atoms configuration

## 2.        Periodic Boundary Conditions (PBC)

For the current study, the periodic boundary conditions were applied to the computational domain such that the number of atoms leave the computational domain is equal to the number of atoms that enter the inlet domain. Due to the fact that the simulated system of molecules geometry is very small, the surface effect has a great influence on the molecular dynamic program performance and calculations, and therefore the periodic boundary conditions were used to reduce the atoms surface effect interaction with the walls [6], [17].

## 3.        Simulation Conditions

The geometry used for performing the required calculations consists of a system of molecules in which the number of atoms is equal to 800 atoms.

16

The simulation conditions used here were similar to the conditions stated in the simulation formulation of the previous section. Periodic boundary conditions were employed and the simulation was conducted for the following cases:

1.       Fluid flow simulation.

2.       Particles-fluid interaction.

3.       Random Particles-fluid interaction.

4.       Simulation of (SLI) with different particles velocities.

In all cases stated above, the $y-direction$ velocity value was equal to zero; this will allow us to observe the system of molecules in the $x-z$ plane only. Finally, the simulation results for different solid particles-fluid interaction formulations are discussed and explained in detail in Chapter V.

THIS PAGE INTENTIONALY LEFT BLANK

# IV. MACRO-SCALE MODEL RESULTS AND DISCUSSION

## A. PARTICLES INJECTION SIMULATION

As in many other commercial finite element analysis programs, the three main processes of the problem analysis discussed in this paper are preprocessing, problem solving and post processing, respectively.

First of all, many computational domains were studied with and without particles injection for the laminar flow. The following case represents a 0.02*m* x 0.2*m* rectangular domain with or without injected particles of 500 microns. The purpose of studying the two different cases is to observe the effect of the particles injection on the fluid.

In the preprocessing stage, CFD geometry was used to create the 2D rectangular computational domain containing water fluid. Aluminum particles were injected through this domain. Both water and aluminum properties are tabulated in Table 1. Then, CFD ACE solver is used to specify the boundary conditions and to solve the problem. Finally, CFD View is used for plotting the results such as the velocity profile.

Table 1.        Material properties

| Material | Property | |
|---|---|---|
| Water | Density $[\rho]$ | $\rho = 1.1614 kg / m^3$ |
| | Viscosity $[\mu]$ | $\mu = 1.85 \times 10^{-5} kg / m - \sec$ |
| | Thermal conductivity $[k]$ | $k = 0.0263 \, w/\text{m - k}$ |
| Aluminum | Density $[\rho]$ | $\rho = 2700 kg / m^3$ |
| | Thermal conductivity $[k]$ | $k = 190 \, w/\text{m - k}$ |

In this study, different injection locations as well as particles diameters were studied. The locations of particles are tabulated in Table 2. In this simulation case, the domain is subjected to the boundary conditions as shown in Figure 3. The boundary conditions are applied to the domain in the following way. The inlet wall has a known temperature $T = 300K$ and the $x$-component uniform inlet velocity $v_x = 0.2m/\sec$ while the outlet wall is insulated $\partial T / \partial n = 0$ along the boundary and the pressure $p = 0$. The upper and lower walls have a constant heat temperature $T = 600K$ .

Table.2        Injectors locations along the y-axis

| Injector number | Coordinates $(x, y, z)$ | Particle velocity $[m/\sec]$ |
|---|---|---|
| 1 | $\left(0, 5 \times 10^{-3}, 0\right)$ | 0.2 |
| 2 | $\left(0, 1 \times 10^{-2}, 0\right)$ | 0.2 |
| 3 | $\left(0, 1.5 \times 10^{-2}, 0\right)$ | 0.2 |
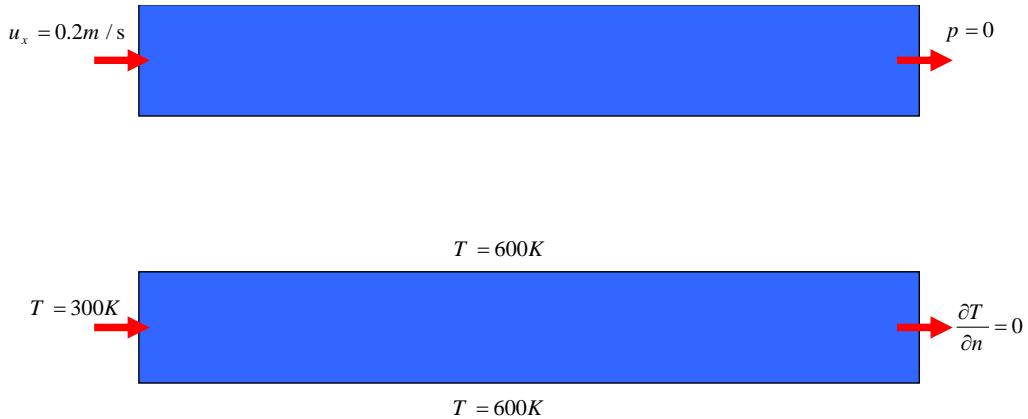


Figure 3.        Boundary conditions

Figures 4 and 5 represent the velocity profile before and after the injection. Figure 4 shows the parabolic profile shape for a fully developed flow at $x = 0.1m$ while Figure 5 indicates how the injected particles can affect the fluid velocity profile. This effect depends on the velocity, the diameter and the injector location.
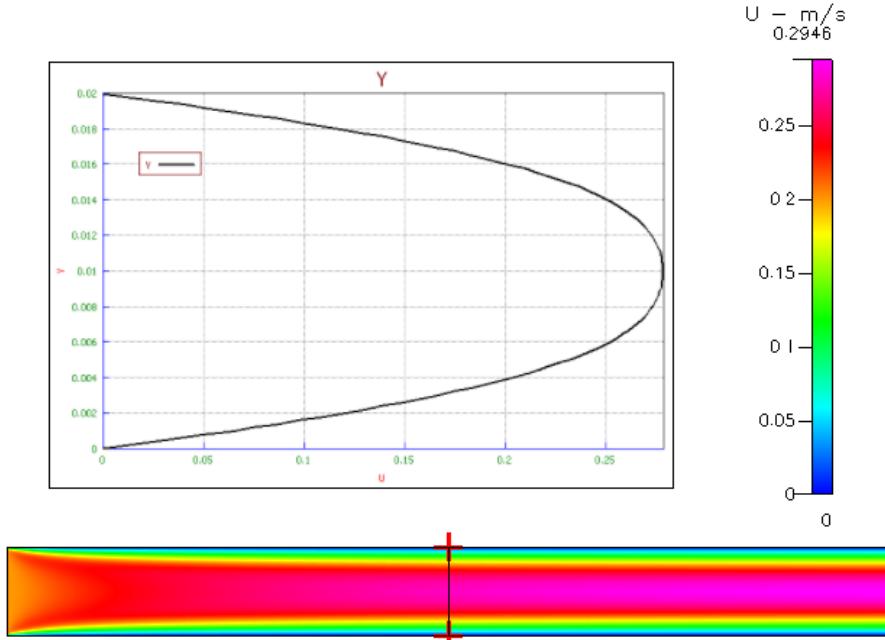


Figure 4.      Velocity profile of fluid at $x = 0.1m$
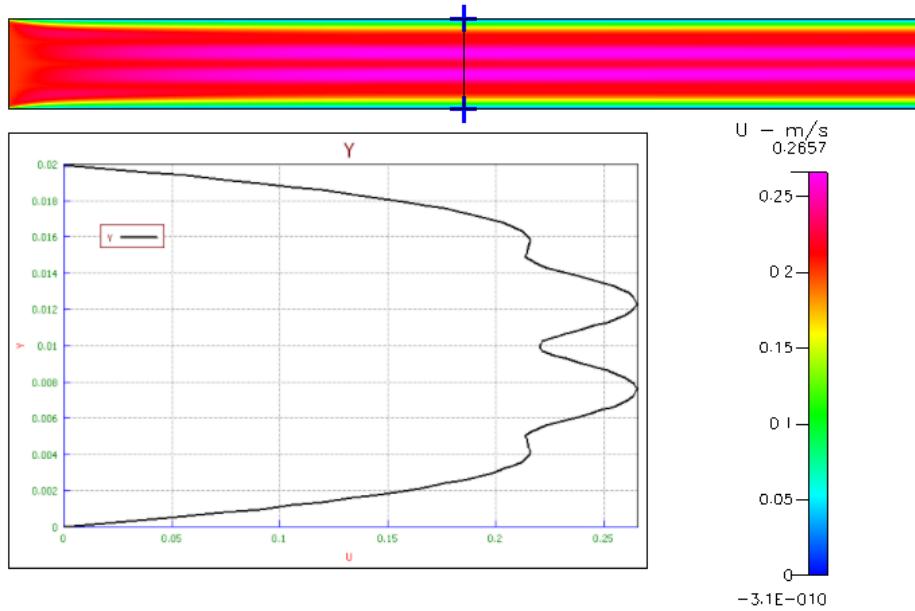


Figure 5.      Velocity profile for the particle injected fluid

Figure 6 represents the trajectory temperature distribution along the domain. By observing the temperature distribution, it is clear that the particles' injected location has a significant effect on the amount of heat the particles can transfer from the domain walls. Therefore, the amount of heat transferred to the fluid will depend on the location and velocity of the particles. As the particles move through the domain, the amount of heat absorbed by the particles will increase. In fact there are several factors that affect the amount of heat transfer along the computational domain, such as the particles location and its diameter.
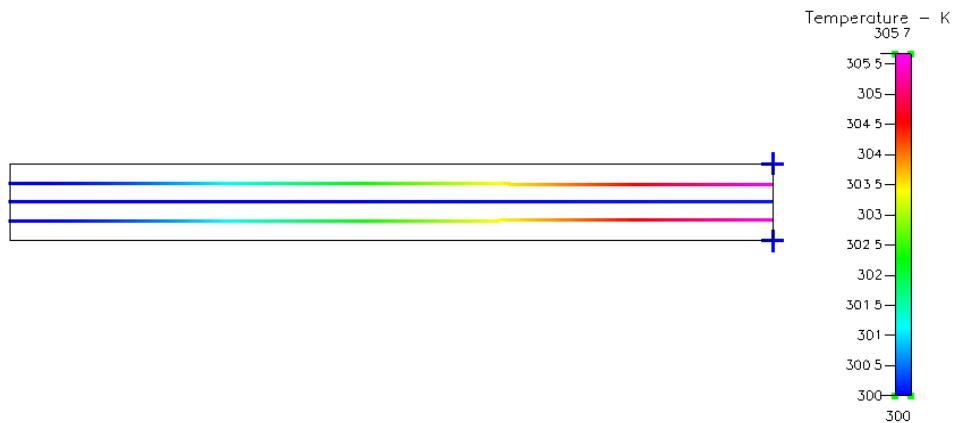


Figure 6.        Particles trajectories temperature distribution

If the diameter of the particles is large enough, the particles will then accumulate at the bottom of the domain and they may end up clogging the pipe/tube. Such a situation must be avoided in the kind of application we studied. This case is shown in Figure 7 for an injected 5000 micron particle having a mass flow rate of $6Kg/\sec$, and in Figure 8 when the particle has a diameter of 50 micron and a mass flow rate of $0.6Kg/\sec$.
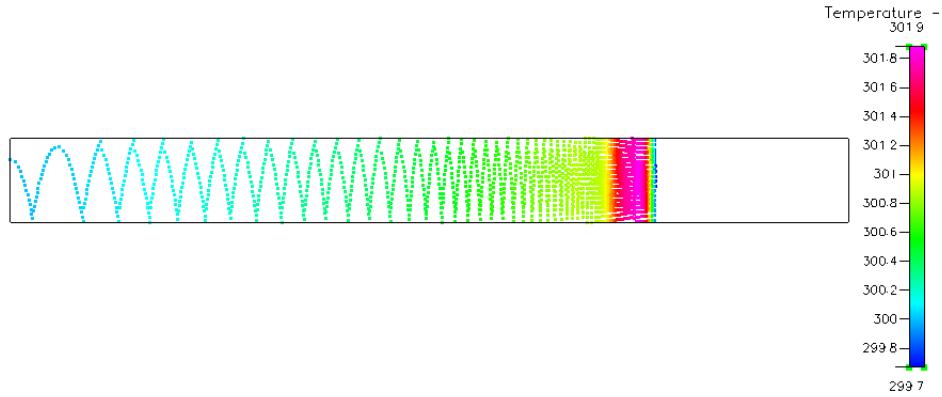
Figure 7.        Clogged pipe
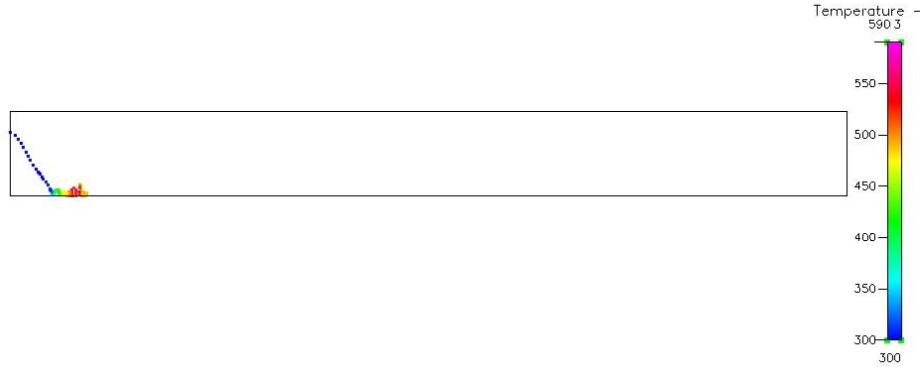


Figure 8.        Accumulation of the particles at the lower wall

By studying different injection simulation situations, it was found that the best particle diameter size in terms of the solver convergence was 0.1 micron, an injected velocity of $1m/s$ for the laminar flow, an inlet velocity of $35m/\sec$ for the turbulence and a mass flow rate of $1\times10^{-3}Kg/\sec$ to simulate our application of interest.

Different simulation cases are studied in the following sections. The first case is for the laminar flow, and the second one is for the turbulent flow. Both cases can be used to study the injection effect on the heat transfer between the wall boundaries. Previous studies have stated that the turbulence is more effective than laminar flow in heat transfer applications. However, the turbulence requires higher velocity than that in laminar flow. As the velocity increases, the time of interaction between the particles and the fluid will

decrease so that there is a limited improvement of the overall heat transfer through the calculation domain. These conditions will be explained in detail in the following sections.

Also in the following sections, different cases of particles injection will be discussed. The particles are injected at different locations in the inlet boundary using a rectangular domain of $0.002m$ x $0.02m$ to simulate the macro-scale model. The boundary conditions used here are still the same as the previously explained case, and the particle diameter used here is 0.1 micron.

In all cases, the particles are maintained to have a velocity similar to the fluid inlet velocity. In order to be able to find the effect of particles injection to enhance the heat transfer properties of the computational domain, the rectangular domain was used to calculate the temperature difference between the outlet and the inlet boundaries with and without any injection for both the laminar flow and the turbulent flow.

The program is used to obtain the velocity profile for both the laminar flow and turbulence. Figure 9 shows that the velocity profile of the laminar flow is fully developed at $x = 0.01m$ and the expected flow parabolic shape is obtained, while Figure 10 shows the turbulence velocity profile. Further discussion about laminar and turbulent flow will be explained in detail in the following sections, and the result obtained here will be used to compare different simulation cases.

It is also necessary to study the pressure distributions along the upper and lower walls to compare it with the injected domain cases. For the laminar flow, the upper and lower walls are subjected to a maximum value of $2.074 \, Pa$ and $2.096 \, Pa$, respectively, as shown in Figures 11 and 12. Figure 13 shows the pressure distribution along the y-axis at $x = 0.01m$ for the laminar flow.

For turbulence, Figures 14 and 15 show that the lower and upper walls are subjected to a pressure with a maximum value of $79,332 \, Pa$ and $79,351 \, Pa$ respectively. Figure 16 shows the pressure distribution along the y-axis at $x = 0.01m$ for the turbulent flow.

The residual plots for both the laminar and turbulent flow indicate that the solution has a 4th order convergence which is accurate enough for the simulation of particles injection/spray. Figures 17 and 18 indicate the solution convergence for the laminar flow and turbulence respectively.
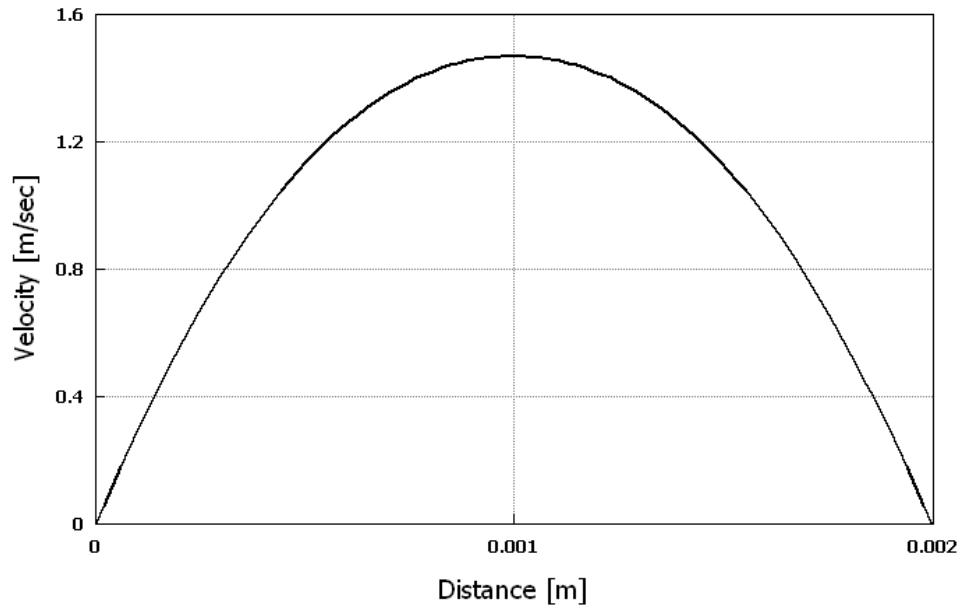


Figure 9.     Laminar flow velocity profile at $x = 0.01m$
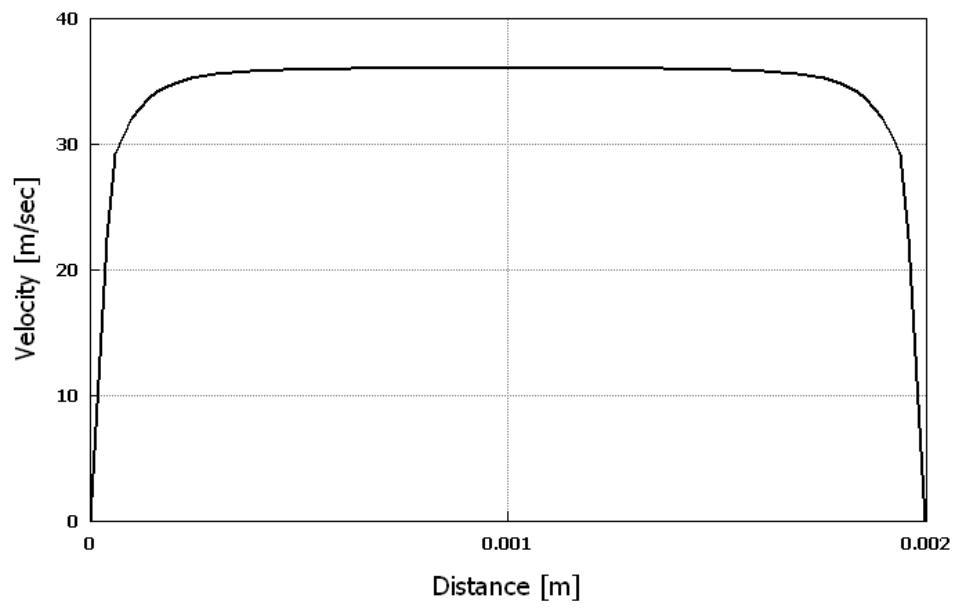
Figure 10.        Turbulence velocity profile at $x = 0.01m$
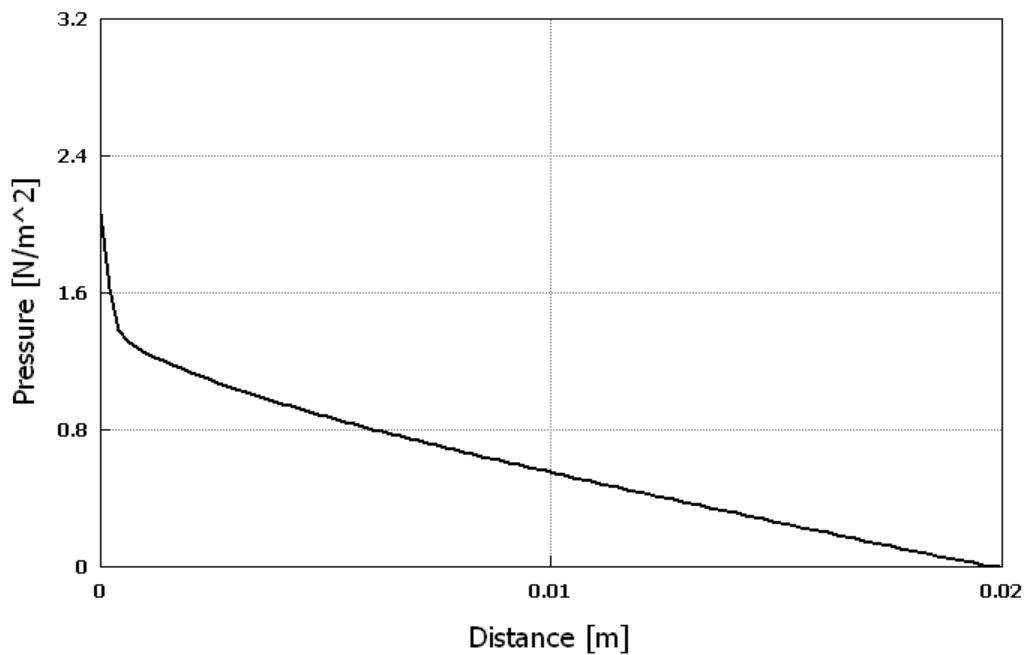


Figure 11.        Laminar flow upper wall pressure distribution
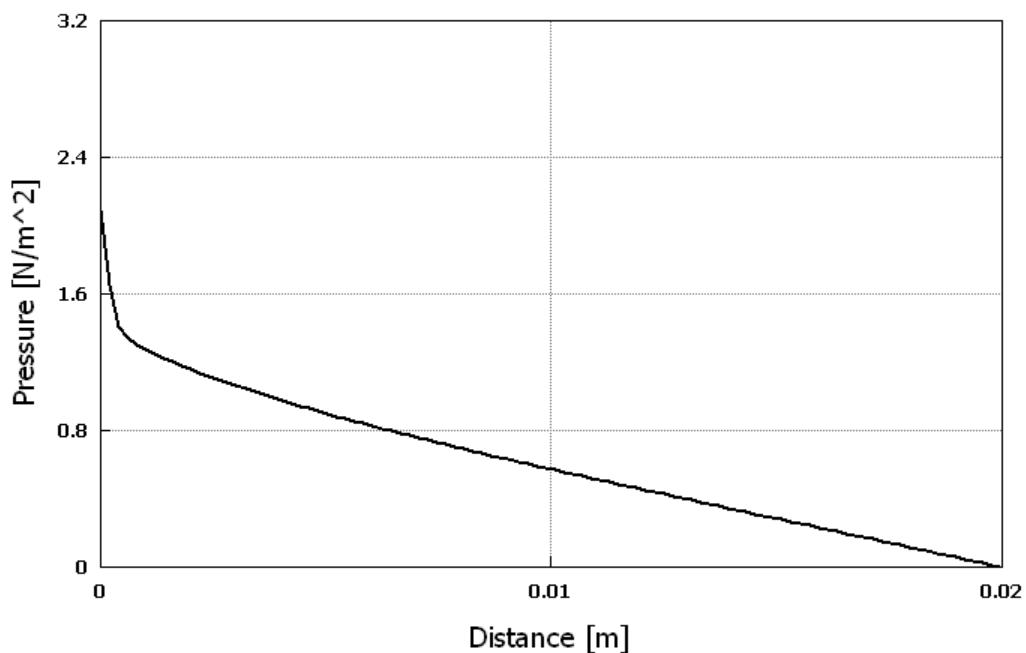
Figure 12.    Laminar flow lower wall pressure distribution
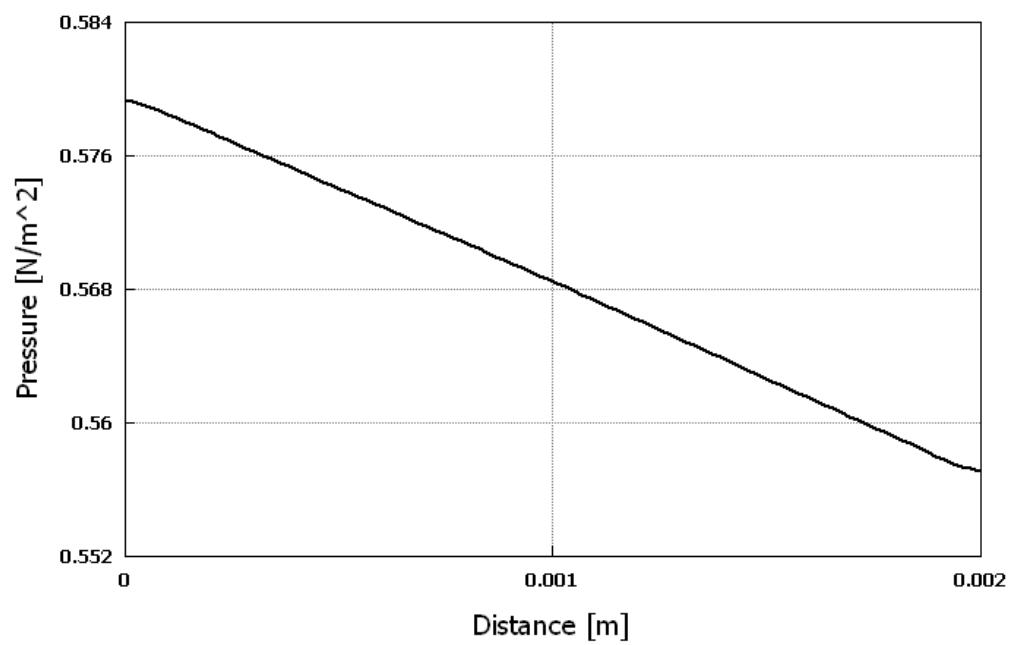


Figure 13.    Laminar flow pressure distribution along the y-axis
at $x = 0.01m$

27
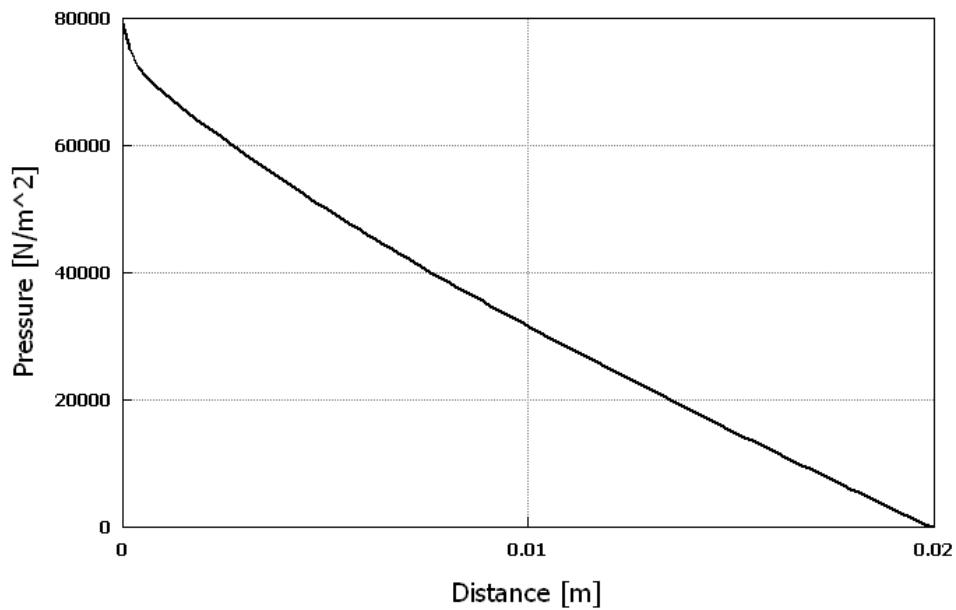
Figure 14.        Turbulence upper wall pressure distribution
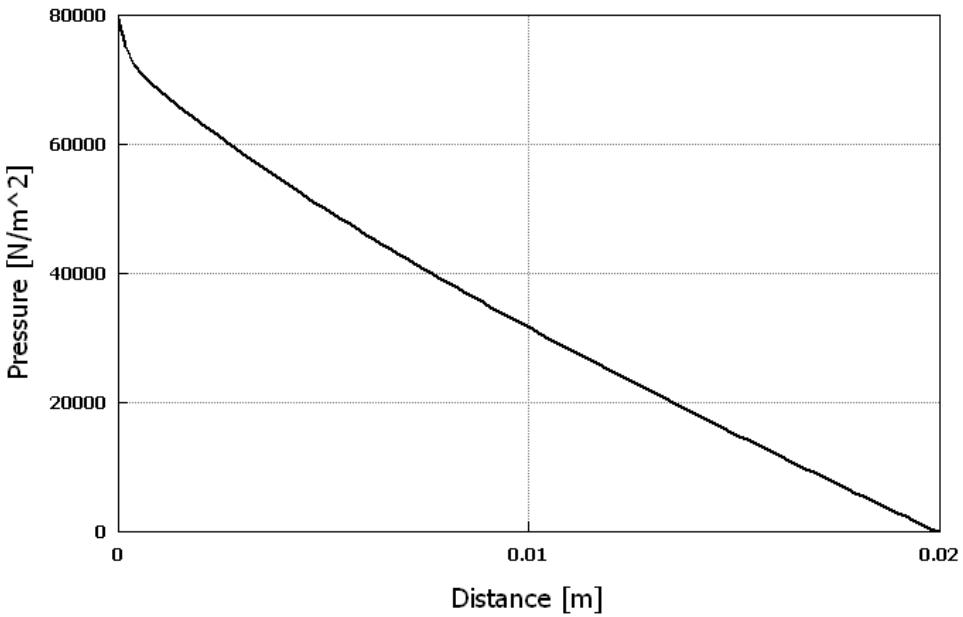


Figure 15.        Turbulence lower wall pressure distribution
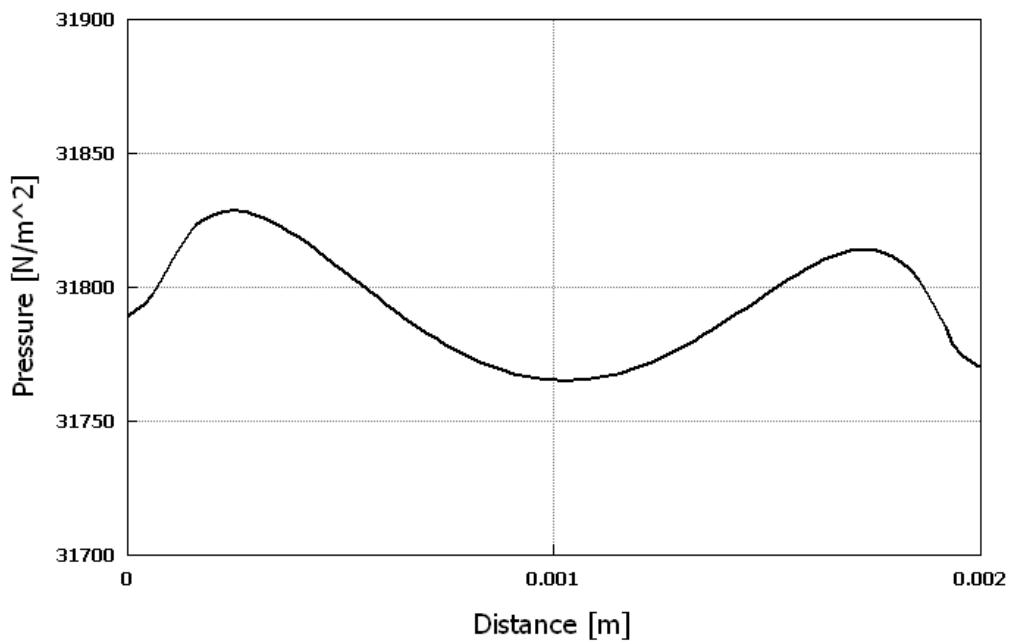
Figure 16.    Turbulence pressure distribution along the y-axis
at $x = 0.01m$
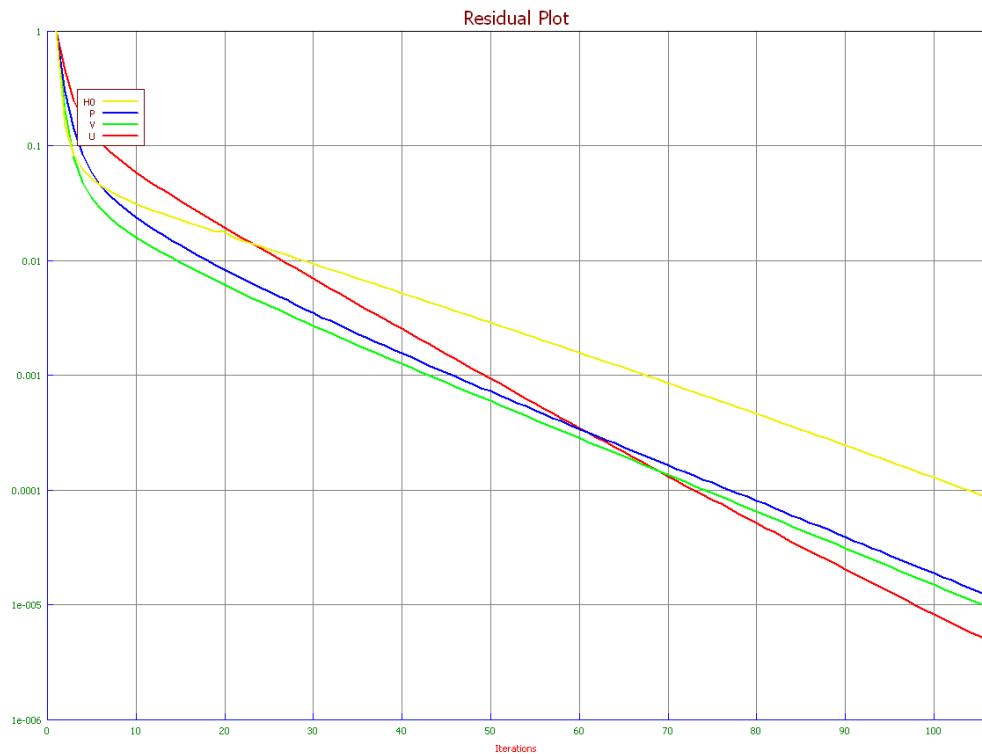


Figure 17.    Residual plot for the laminar flow

29
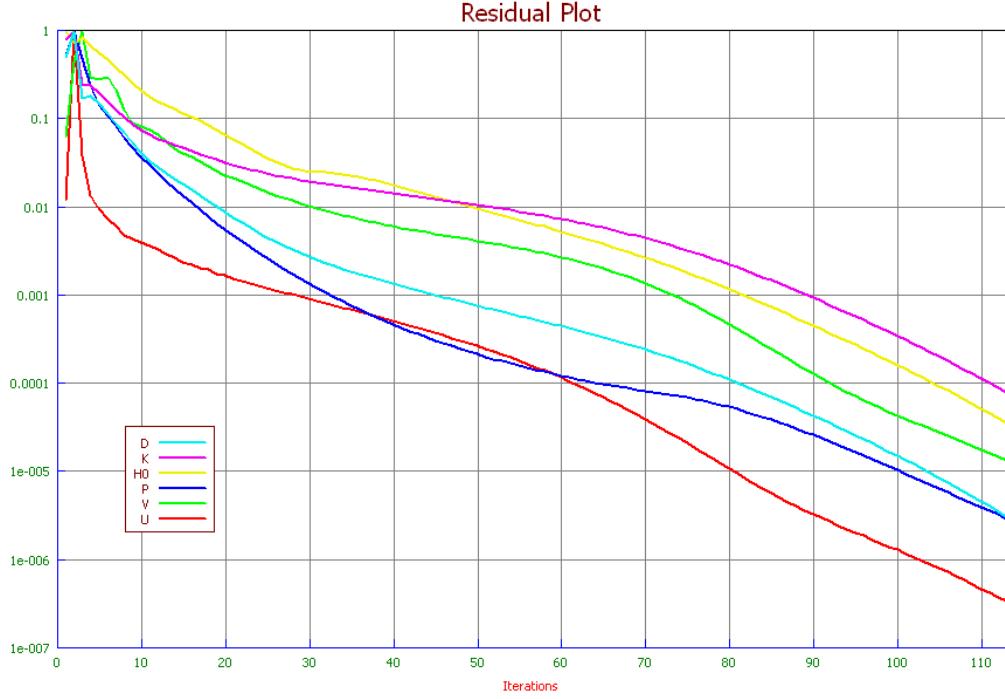
Figure 18.      Residual plot for the turbulent flow

### 1.      Laminar Flow Particles Injection

Again the same computational domain is used with the activation of the spray module option in the program. Injector locations are chosen in three different locations as follows: the first simulation case has an injector located at $\left(0,19.5\times10^{-4},0\right)m$ while the second case has an injector located at $\left(0,1\times10^{-3},0\right)m$. The boundary conditions are maintained the same as before, and the mass flow rate is fixed at $\dot{m}=10^{-3}\,kg\,/\sec$.

### 2.      Turbulence Particles Injection

In order to be able to run the simulation for this case using the same domain to perform the required analysis, it's necessary to generate a turbulent flow using a higher Reynolds number which can be calculated from equation (1.2). Table 3 summarizes the

Reynolds numbers for various fluid inlet velocities. The transition flow range is given by $2000 <$ Reynolds number $> 4000$ [11].

It is clear that the turbulent flow will start to develop at fluid velocity $\geq 15 m/\sec$. Once again, these velocities are very high and it will affect the interaction time between the fluid and the injected particles. The discussion of the results is explained in the following sections. Other than the fluid velocity, the same conditions used for the laminar flow are used.

Table 3.        Reynolds number for different velocities

| Velocity $[m/s]$ | Reynolds number | Flow type |
|---|---|---|
| 5 | 627.8 | Laminar |
| 10 | 1255.6 | Transition |
| 15 | 1833.3 | Transition |
| 20 | 2511.1 | Transition |
| 25 | 3138.9 | Transition |
| 30 | 3766.7 | Transition |
| 35 | 4394.5 | Turbulence |

### B.    HEAT TRANSFER

#### 1.    Laminar Flow

The results of the three cases stated in chapter II are tabulated below in Table 4. From the table, it's clear that the injector located at the middle of the inlet boundary has a larger temperature difference between the inlet and outlet walls. The overall heat transfer increase is found to be equal to 3.7%, which is not large. The reason why the obtained result was low is related to the particles' diameter as well as the small amount of the mass

flow rate that we have used due to the limitation in the size of the domain, as discussed previously in Chapter II. Considering such a small mass flow rate of microscale particles, the increase of heat transfer due to the particles is notable. An alternative solution will be using more than one injector to improve the working fluid heat properties, but unfortunately this can not be performed in the available CFD+ multiphysics program.

Table 4.        Laminar flow heat transfer summary along the domain

| Injector Location $(x,y,z)$ | Mass flow rate $[kg\,/\,s]$ | Heat transfer $[watts\,/\,m]$ | | | Increased heat transfer ratio |
|---|---|---|---|---|---|
| | | Inlet | Outlet | Outlet-Inlet | |
| N/A | 0 | 688.92 | 1143.9 | 454.98 | 1.00 |
| $(0,19.5\times10^{-4},0)$ | $1\times10^{-3}$ | 688.80 | 1159.0 | 470.2 | 1.033 |
| $(0,1\times10^{-3},0)$ | $1\times10^{-3}$ | 688.93 | 1161.1 | 472.17 | 1.037 |

### 2.        Transition Flow

The simulation was performed again for the same boundary conditions used before but the inlet velocity was changed. Table 5 shows the result obtained from CFD + ACE multiphysics program.

From the table, it can be noticed that the heat transfer potential will increase as the fluid inlet velocity increases, but the injection effect will not enhance the domain heat transfer.

Table 5.    Laminar flow heat transfer summary along the domain

| $v_x$ [m/sec] | Injector Location $(x,y,z)$ | Mass flow rate $[kg/s]$ | Heat transfer $[watts/m]$ | | | Increased heat transfer ratio |
|---|---|---|---|---|---|---|
| | | | Inlet | Outlet | Outlet-Inlet | |
| 10 | N/A | 0 | 7014.7 | 8268.3 | 1253.6 | 1.00 |
| 10 | $(0, 19.5 \times 10^{-4}, 0)$ | $1 \times 10^{-3}$ | 7014.7 | 8271.3 | 1256.6 | 1.002 |
| 20 | N/A | 0 | 14033 | 15777 | 1744 | 1.00 |
| 20 | $(0, 19.5 \times 10^{-4}, 0)$ | $1 \times 10^{-3}$ | 14033 | 15779 | 1746 | 1.001 |
| 25 | N/A | 0 | 17542 | 19488 | 1946 | 1.00 |
| 25 | $(0, 19.5 \times 10^{-4}, 0)$ | $1 \times 10^{-3}$ | 17542 | 19490 | 1948 | 1.001 |

**3.    Turbulence**

Repeating the same procedures used before for the laminar flow yields results for the turbulent flow indicated in Table 6. It can be noticed that the particles injection doesn't affect the overall heat transfer difference between the inlet and the outlet boundaries. In fact, the heat transfer was decreased in the second case as shown in the table.

As expected, turbulent flow improves the heat transfer properties of the domain compared to the laminar flow.  However, the injection is more effective for the laminar flow, as explained in the previous section. In order to generate more effective turbulent flow, many useful methods can be used but we are limited here by the small size of the nanotechnology applications, and therefore most of the known cases are not useful here.

Table 6.          Turbulence heat transfer summary through the domain
$$\left(v_x = 35m/s\right)$$

| Injector Location $(x, y, z)$ | Mass flow rate $[kg/s]$ | Heat transfer $[watts/m]$ | | | Increased heat transfer ratio |
|---|---|---|---|---|---|
| | | Inlet | Outlet | Outlet-Inlet | |
| Nil | 0 | $8.749 \times 10^7$ | $8.945 \times 10^7$ | $2.05 \times 10^6$ | 1.0 |
| $\left(0, 19.5 \times 10^{-4}, 0\right)$ | $1 \times 10^{-3}$ | $8.749 \times 10^7$ | $8.955 \times 10^7$ | $2.05 \times 10^6$ | 1.0 |
| $\left(0, 1 \times 10^{-3}, 0\right)$ | $1 \times 10^{-3}$ | $8.749 \times 10^7$ | $8.955 \times 10^7$ | $1.96 \times 10^6$ | 0.95 |

## C.    PRESSURE DISTURBUTION ALONG THE DOMAIN

By observing the velocity profile of the previous cases, it's important to investigate in detail the pressure distribution along the computational domain to inspect the working fluid behavior and to study the effect of the pressure associated with the particles injection/spray to avoid any pipe/tube vibration.

First of all, the steady state simulation is used to study the pressure distribution along the domain at different injector's locations as indicated in Table 7. These coordinates were chosen to investigate the pressure caused by the injection at different injection locations.  After that, the steady state simulation is performed again for each case, and the results are discussed in the following sections.

Table 7.　　　　Injector's different locations

| Case No. | Injector Location $(x, y, z)$ |
|----------|-------------------------------|
| 1 | $\left(0, 1\times10^{-4}, 0\right)$ |
| 2 | $\left(0, 4\times10^{-4}, 0\right)$ |
| 3 | $\left(0, 6\times10^{-4}, 0\right)$ |
| 4 | $\left(0, 1\times10^{-3}, 0\right)$ |

**1.　　Laminar Flow Steady State Simulation**

The cases indicated in Table 6 are used to obtain the velocity profile and the pressure distributions at the lower and upper walls along the domain. Figures 19, 20 and 21 plot the laminar flow velocity profile, pressure distribution at the upper wall and the pressure distribution at the lower one, respectively, for the first case.  Figure 19 shows how the velocity profile changed due to the injection near the lower wall. Figure 20 indicates that the upper wall is subjected to a maximum pressure of  $1.525\ Pa$  while the lower wall is subjected to a maximum pressure of  $5.541\ Pa$  as shown in Figure 21 below.  Figure 22 shows the pressure distribution along the y axis at $x = 0.01m$. After that a series of simulations were performed again, and the velocity profiles for the other cases are shown in Appendix A.
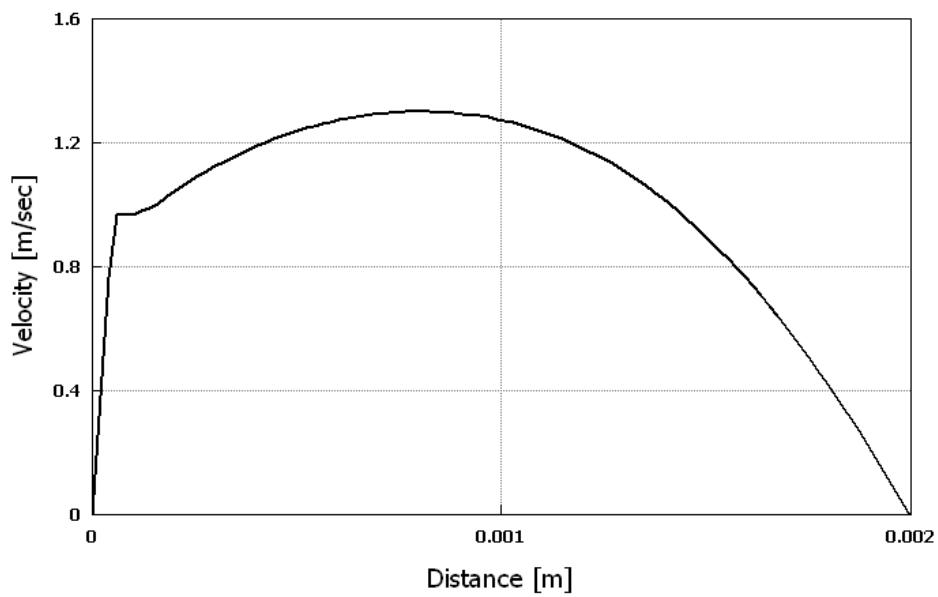
Figure 19.    Laminar flow injected domain at $y = 1 \times 10^{-4} m$ velocity profile
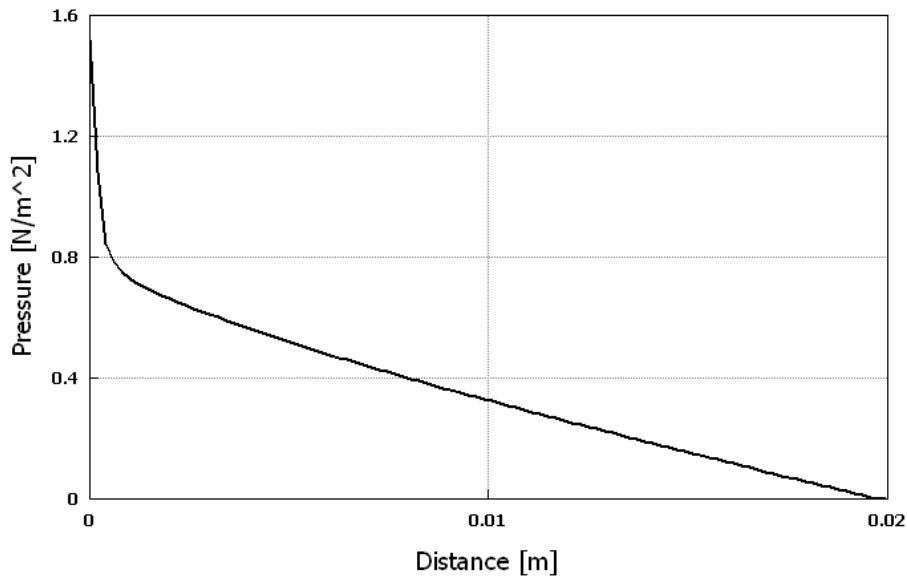


Figure 20.    Laminar flow upper wall pressure distribution (Case no.1)
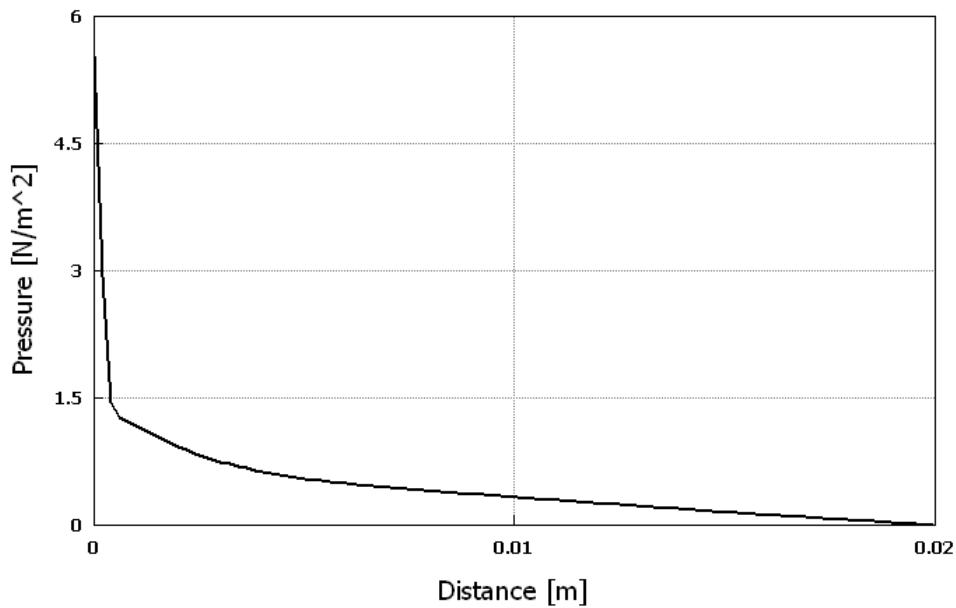
Figure 21.       Laminar flow lower wall pressure distribution (Case no.1)
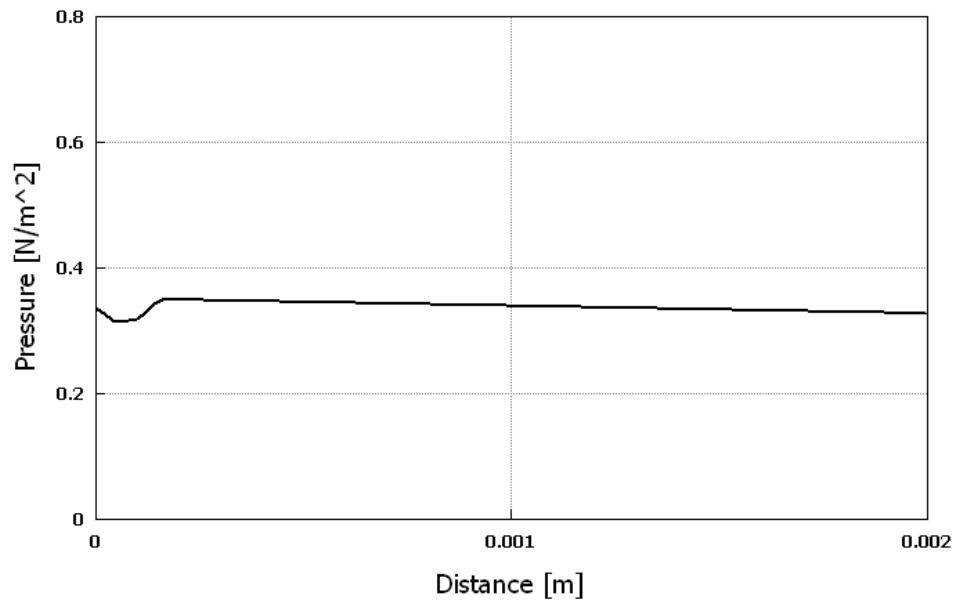


Figure 22.       Laminar flow pressure distribution along y-axis

The maximum pressure values are tabulated in Table 8. It can be observed from the table that there is a significant pressure difference between the walls for all cases except the injector located at the center of the domain. The pressure increase in all

injected cases was compared to the one without any particles injection.     Figure     23
shows the normalized pressure for all previous cases compared to the case without any
injection. A higher pressure at the walls resulting from particle injections will result in a
larger magnitude of fluid structure interaction if the wall is not rigid.  This will cause a
greater potential for structural failure.

Table 8.        Laminar flow maximum pressure at the upper and lower walls

| Case No. | Upper wall pressure $\left(N/m^2\right)$ | Lower wall pressure $\left(N/m^2\right)$ |
|----------|-----------------|-----------------|
| No injection | 2.07 | 2.096 |
| 1 | 1.525 | 5.5416 |
| 2 | 2.429 | 4.016 |
| 3 | 2.895 | 3.610 |
| 4 | 3.077 | 3.108 |
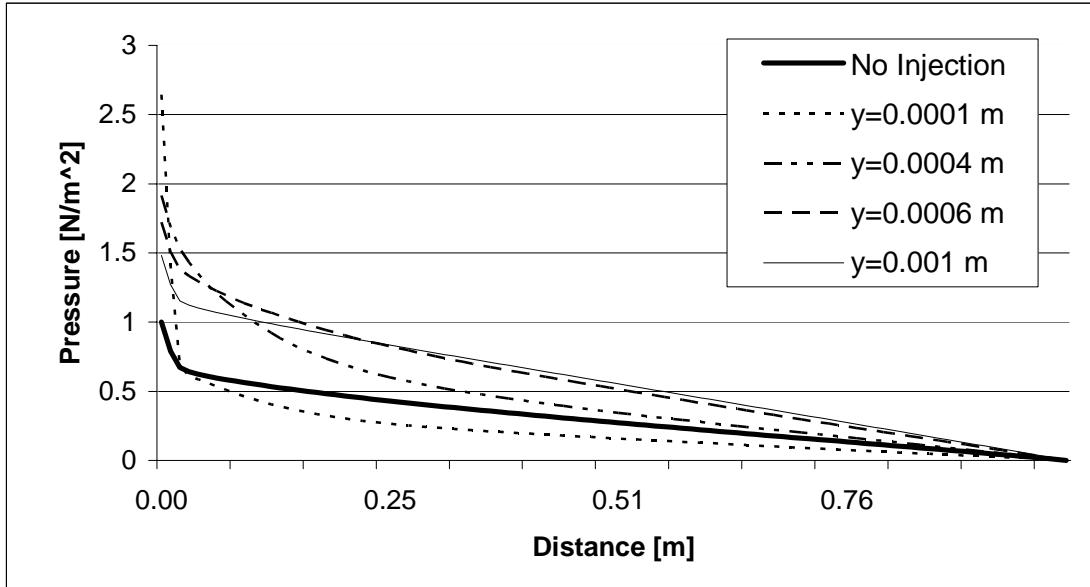


Figure 23.      Laminar flow normalized pressure at lower wall for the all
cases

Further investigation is carried out by changing the particle mass flow rate of the injected particles at different locations along the *y-axis*. Figure 24 shows the normalized pressure at the lower domain wall for different mass flow rates injected at the center of the inlet domain compared to the original case without any particles injection. It can be concluded from this figure that there is a huge pressure difference caused by the injection. However, the higher the mass flow rate is, the lower is the pressure variation. It is more practical to use a higher mass flow rate as much as possible because of the reduction in the pressure variation which will reduce the pipe/tube vibration. It can be also noticed that the pressures variation caused by the mass flow rates of $\dot{m} = 1 \times 10^{-1} Kg / \sec$ and $\dot{m} = 1 Kg / \sec$ are identical for both cases.
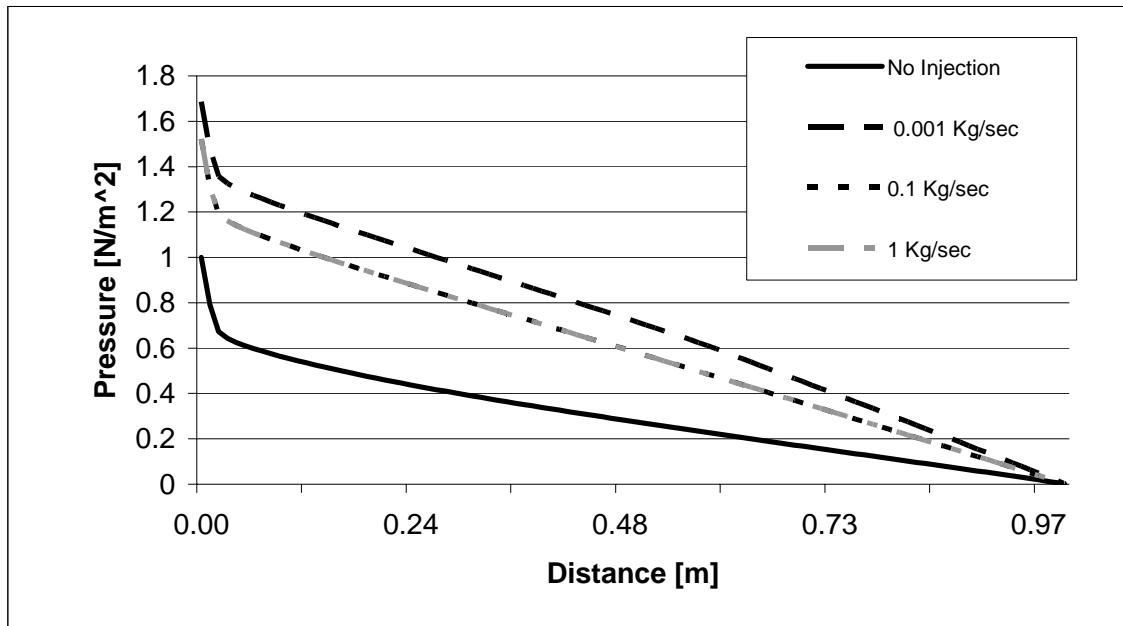


Figure 24.    Laminar flow normalized pressure at lower wall for
different particle mass flow rates at the center of the inlet domain

The effect of mass flow rates is investigated again at $y = 6*10^{-3} m$ . In this case, as shown in Figure 25 below, a higher particle mass flow rate resulted in a much higher

pressure along the wall. Comparing Figures 23 and 24 indicates that the effect of mass flow rate is more significant for the particle injection away from the center of the channel.
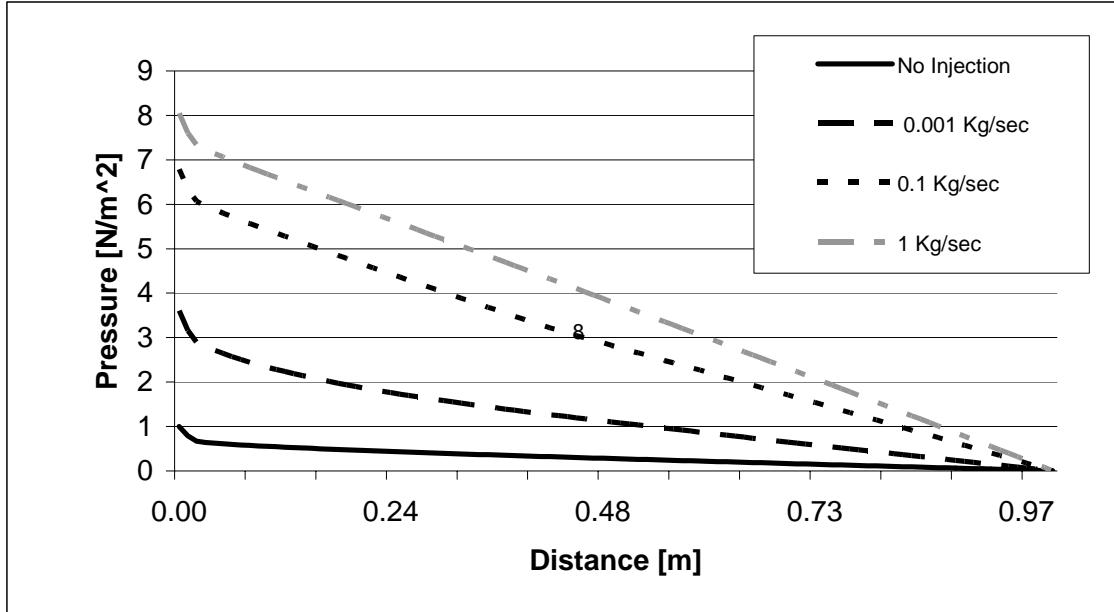


Figure 25.    Laminar flow normalized pressure at lower wall for different mass flow rates at $y = 6x\,10^{-3}\,m$

## 2.    Turbulent Flow Steady State Simulation

Again the simulation is performed for the same cases as the laminar flow, and the results of the maximum pressure at the walls are tabulated below in Table 9.  The results show that the injection has no significant effect on the pressure distribution. In some cases as noticed in the table, the pressure is reduced.  It can be concluded that the injection has no critical effect on the pipe/tube vibration for the turbulent flow.

Similar to the laminar flow, the same cases are used to obtain the velocity profile and the pressure distributions at the lower and upper walls along the domain. Figure 26 shows the turbulence normalized pressure at the lower wall while Figures 27, 28 and 29 represent the turbulent flow velocity profile, pressure distribution at the upper wall and the pressure distribution at the lower one respectively for the first case.  Figure 30 shows

that the injection has a minor effect on the pressure profile. A series of additional simulations were performed again, and the velocity profiles for the other cases are shown in Appendix B.

Table 9.        Turbulent flow maximum pressure at the upper and lower walls

| Case No. | Upper wall pressure $(N/m^2)$ | Lower wall pressure $(N/m^2)$ |
|---|---|---|
| No injection | 79332.6 | 79351.6 |
| 1 | 79332.5 | 79398.3 |
| 2 | 79305.9 | 79344.2 |
| 3 | 79331.5 | 79356.7 |
| 4 | 79332.5 | 79357.5 |
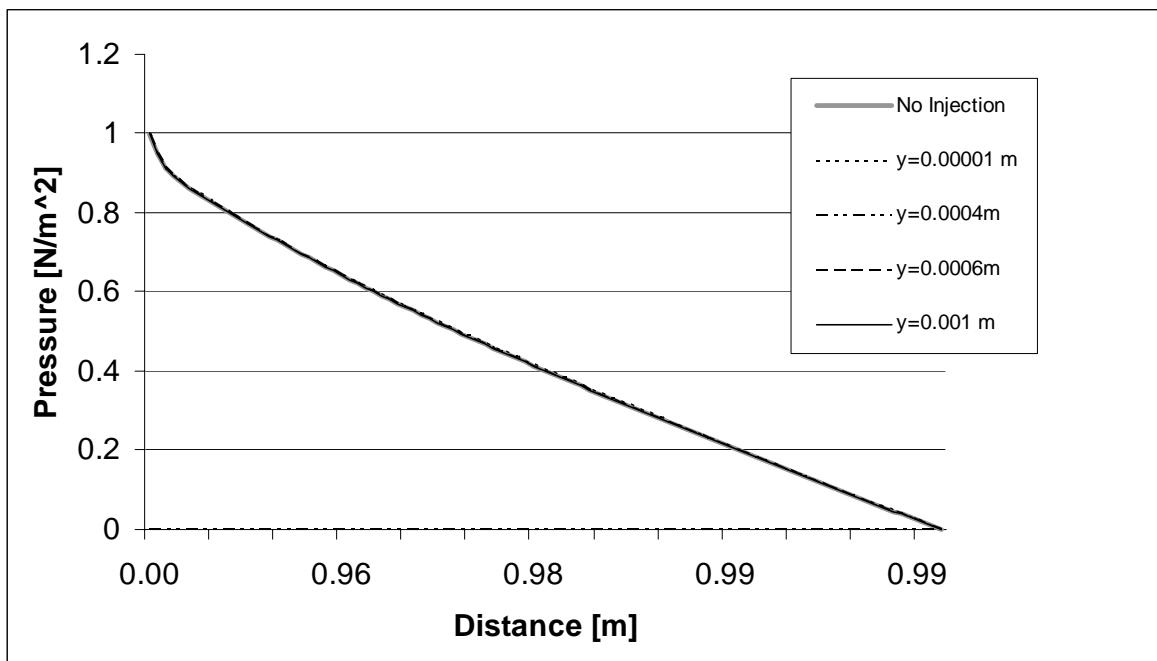


Figure 26.        Turbulence normalized pressure at lower wall for the all cases
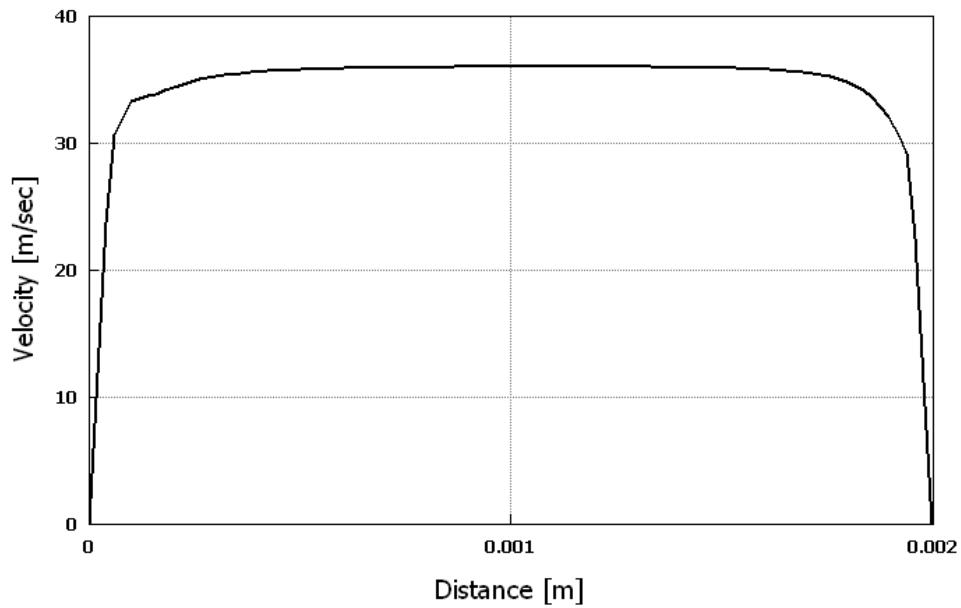
Figure 27.    Turbulence injected domain at $y = 1 \times 10^{-4} m$ velocity profile
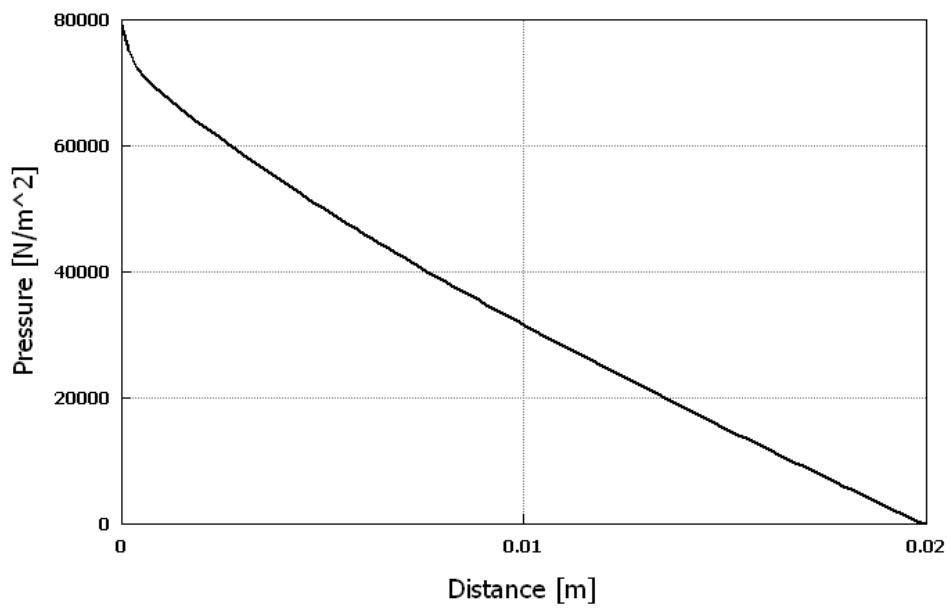


Figure 28.    Turbulence upper wall pressure distribution (Case no.1)
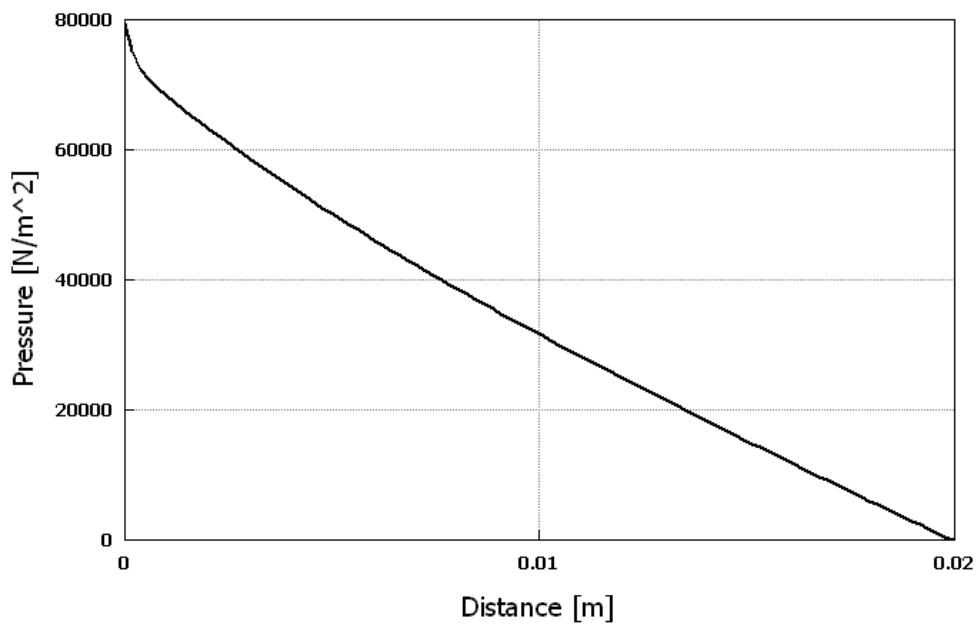
Figure 29.        Turbulent flow lower wall pressure distribution (Case no.1)
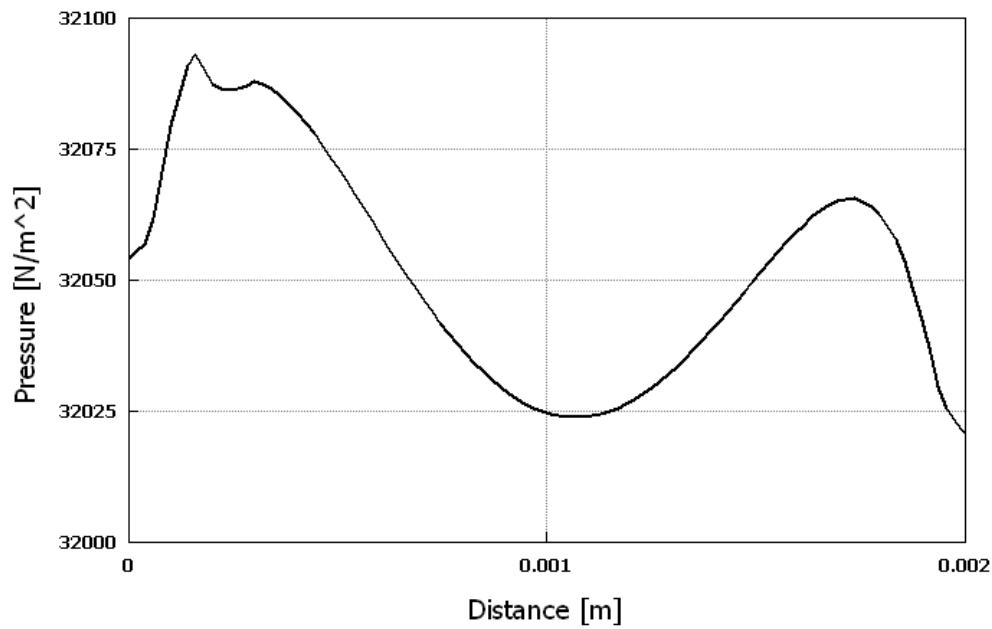


Figure 30.        Turbulence pressure distribution along y-axis

43

THIS PAGE INTENTIONALLY LEFT BLANK

# V. NANO-SCALE MODEL RESULTS AND DISCUSSION

Different simulation cases were conducted. First of all the behavior of the fluid flow through the computational domain was studied. Then the same domain was used to study the effect of the solid particles on the fluid flow and to compare it to the results obtained in Chapter IV.

## A. FLUID FLOW SIMULATION

The simulation was performed to obtain the velocity profile of the flow at different locations along the $x-axis$. In this section the liquid atoms only have an assigned $x-direction$ velocity by applying the force $f_{xf} = 0.1$ along the $x-direction$.
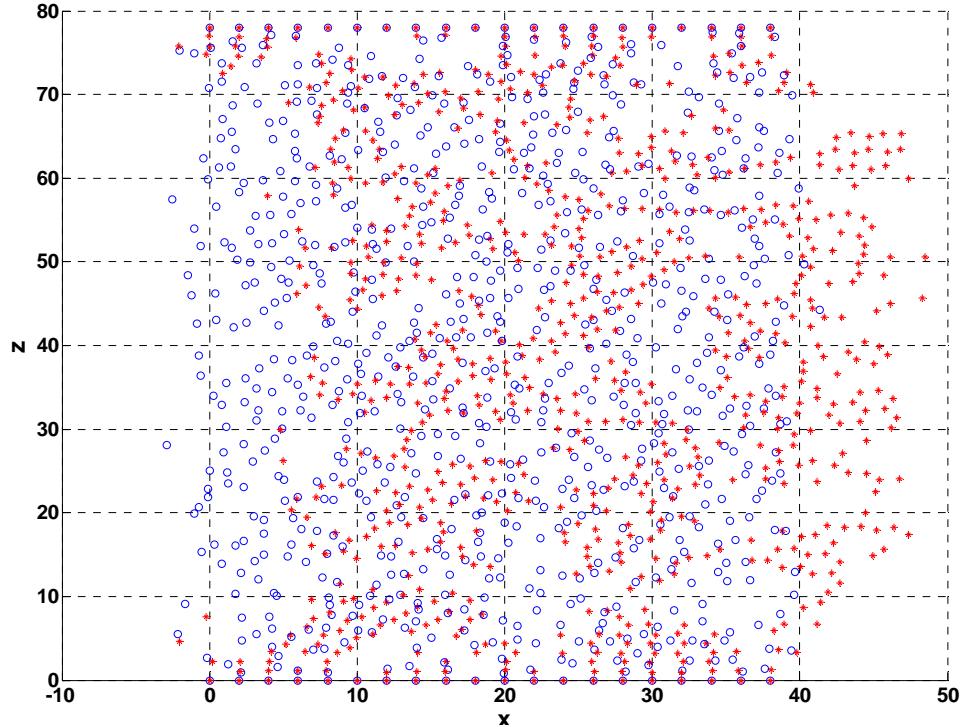


Figure 31.    Original and final atoms configurations with $f_{xf} = 0.1$

Figure 31 shows that the liquid atoms have a significant amount of motion compared to the other solid atoms located near the upper and lower walls while Figures 32 - 35 show the velocity profile at $x = 4, \ 20, \ 32,$ and 37 respectively.
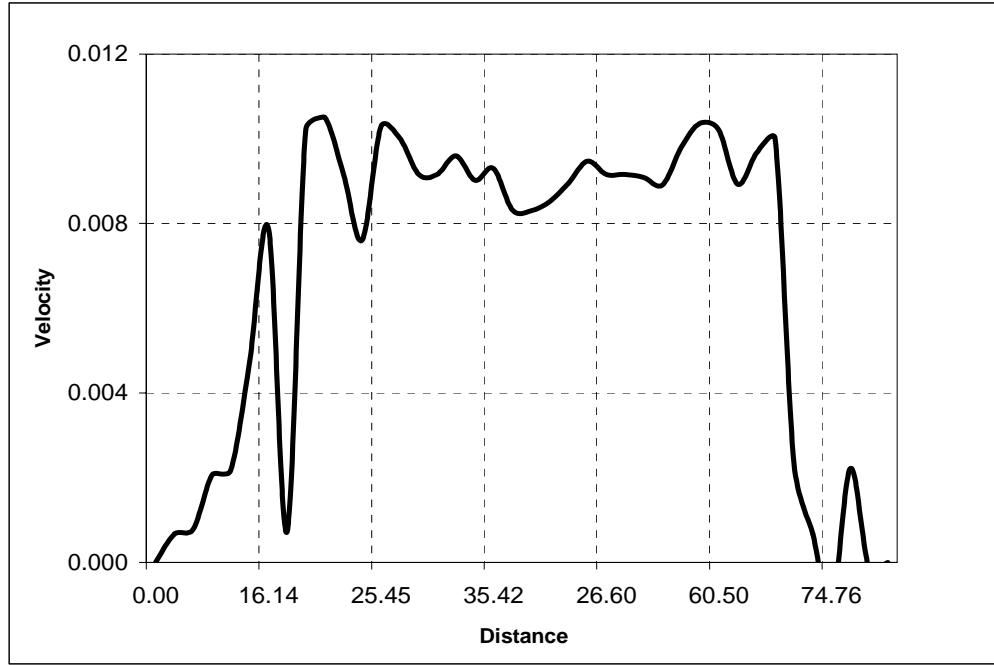


Figure 32.    $X-direction$ velocity profile at $x = 4$

Figure 32 indicates that the velocity profile is somewhat similar to most of the velocity profiles obtained at the inlet of the computational domain. This figure shows that the solid atoms have a small amount of motion compared to the fluid atoms.

However, in this case it is expected to have fluctuation in the profile due to the atoms' vibration when simulation is performed at an atomic level. Figures 34 and 35 show that the flow profile is gradually developed until the velocity profile somewhat similar to the expected parabolic shape is obtained at $x = 37$ (Figure 35).
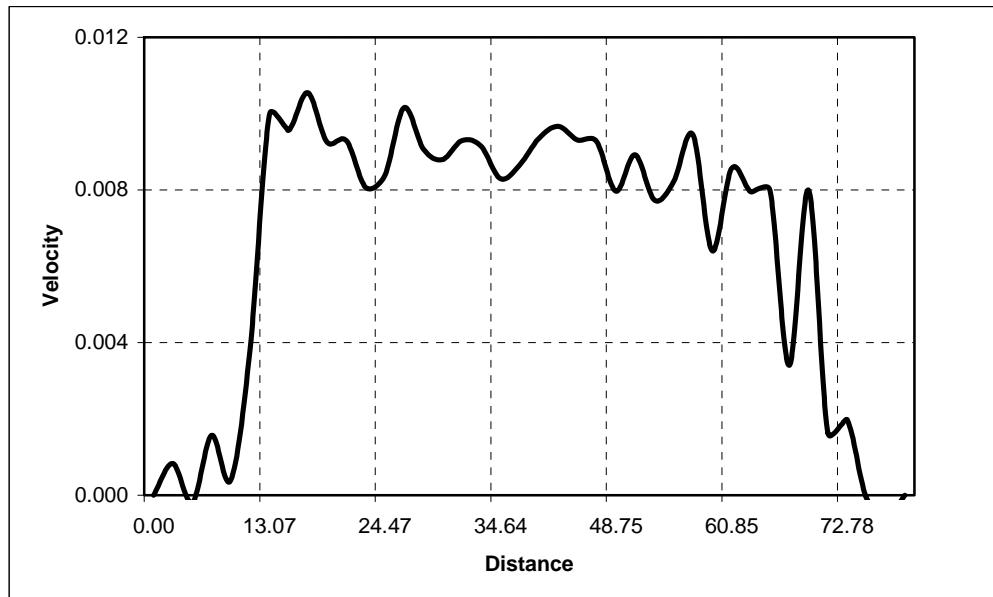
Figure 33.      $X-direction$ velocity profile at $x=20$
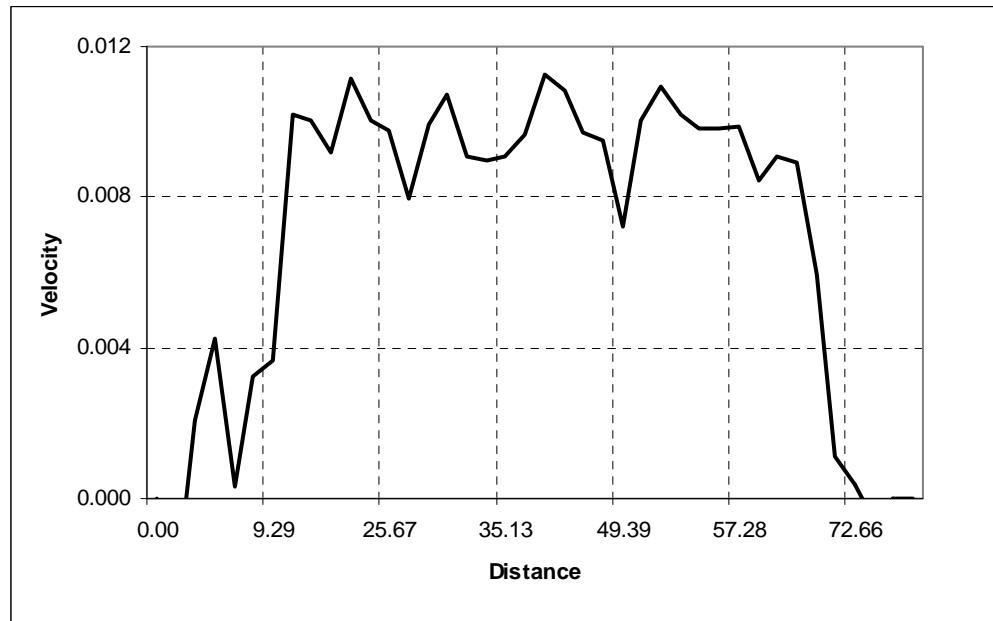


Figure 34.      $X-direction$ velocity profile at $x=32$
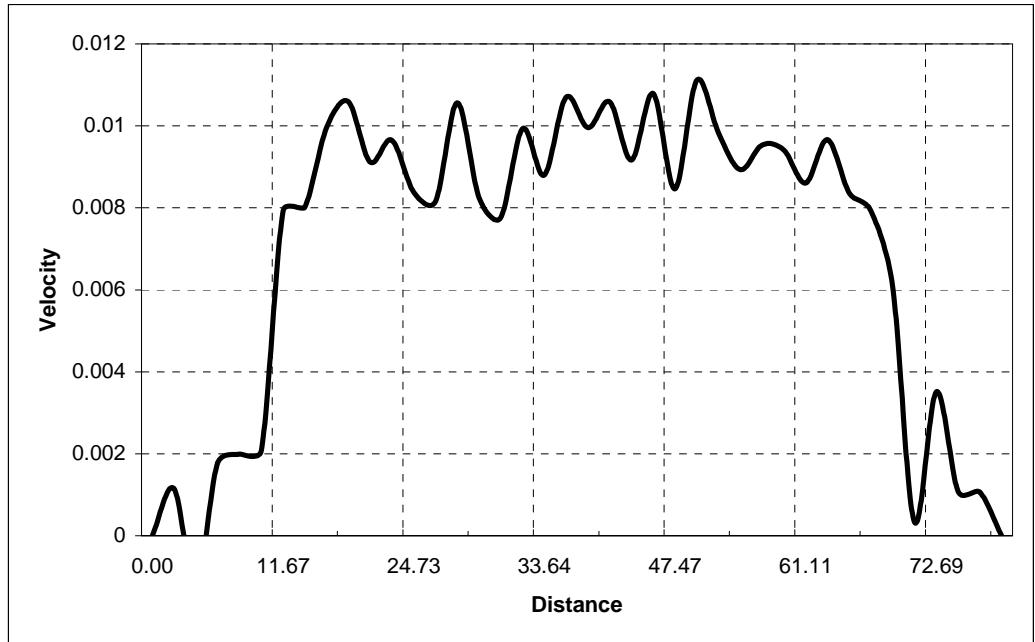
Figure 35.    *X − direction* velocity profile at $x = 37$

## B.    PARTICLES-FLUID INTERACTION

Different simulation cases were performed for the particle fluid injection to study the effect of these particles on the fluid behavior.

### 1.    Horizontal Solid Particles-Fluid Interaction

This case is identical to the previous section but some internal atoms were chosen as solid atoms while the other atoms were maintained as fluid atoms. The locations of the solid atoms are shown in Figure 36.
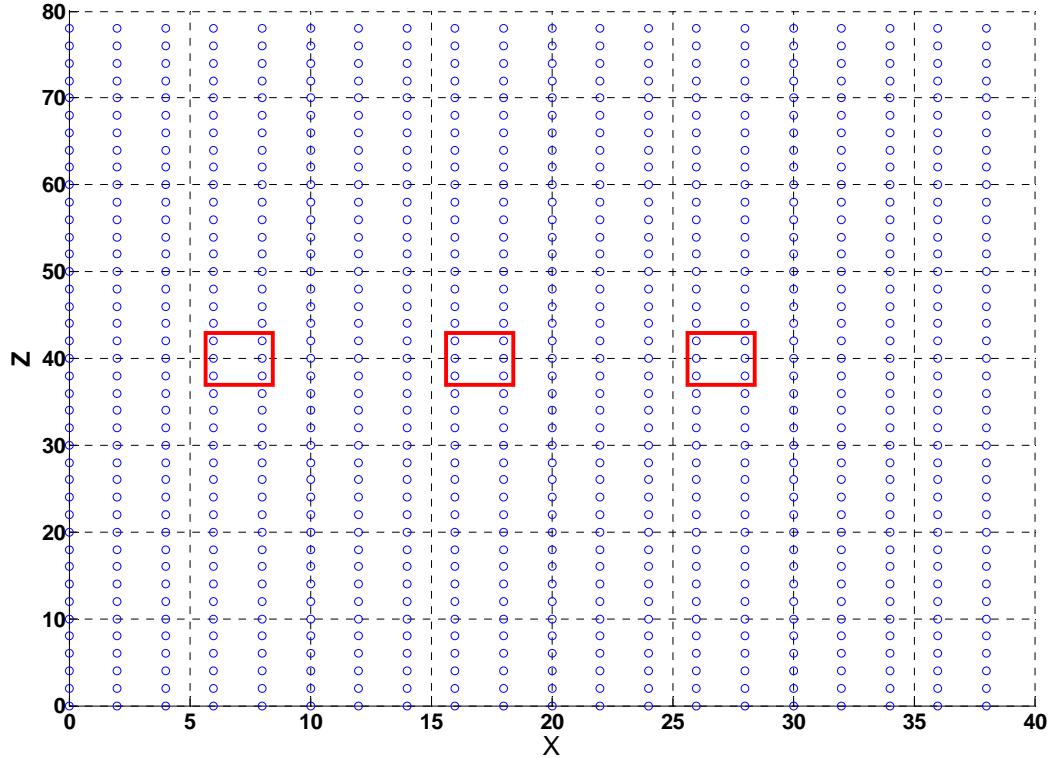
Figure 36.        Solid atoms locations

Figure 37 represents the original solid atoms' configuration and the final atoms' configurations after running the simulation for 10000 iterations.   Comparing this configuration with the one obtained in the previous section, the change in the atoms' configuration can be observed; however, it is difficult to indicate the difference between the two figures.

By tracking the first set of the horizontal particles, it is clear that the solid atoms have a small amount of motion, as expected, compared to that in liquid atoms of the previous section case (see Figures 38, 39).
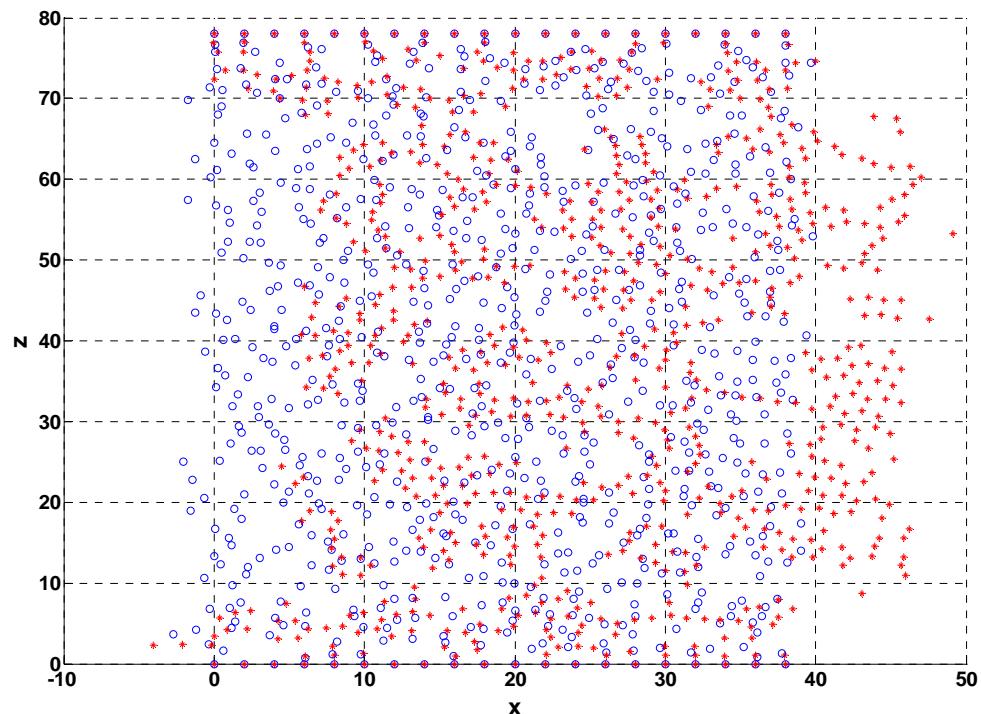
Figure 37. Solid-liquid atoms configurations
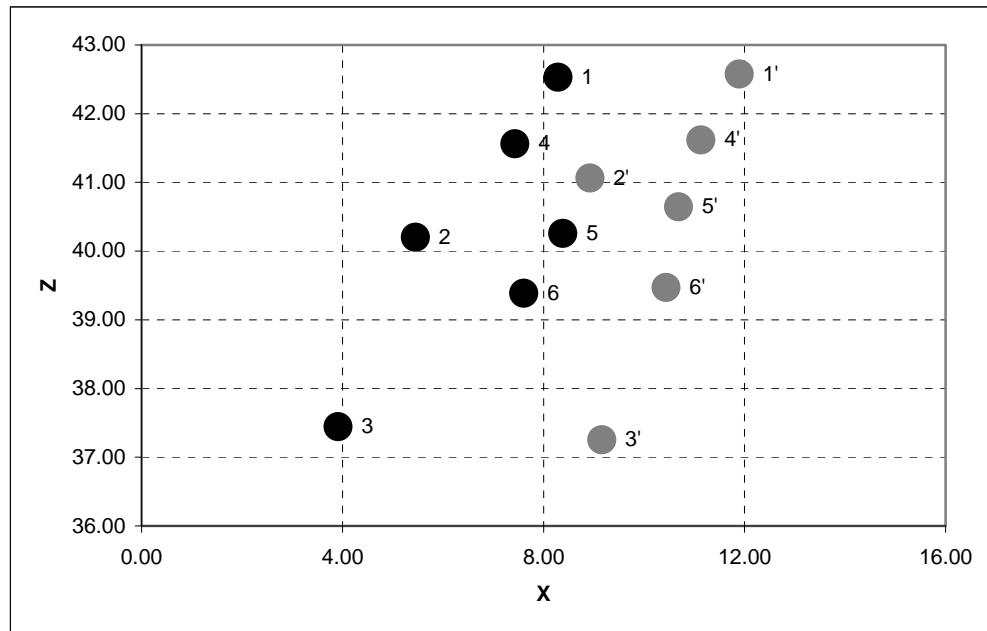


Figure 38. Solid atoms original and final configurations
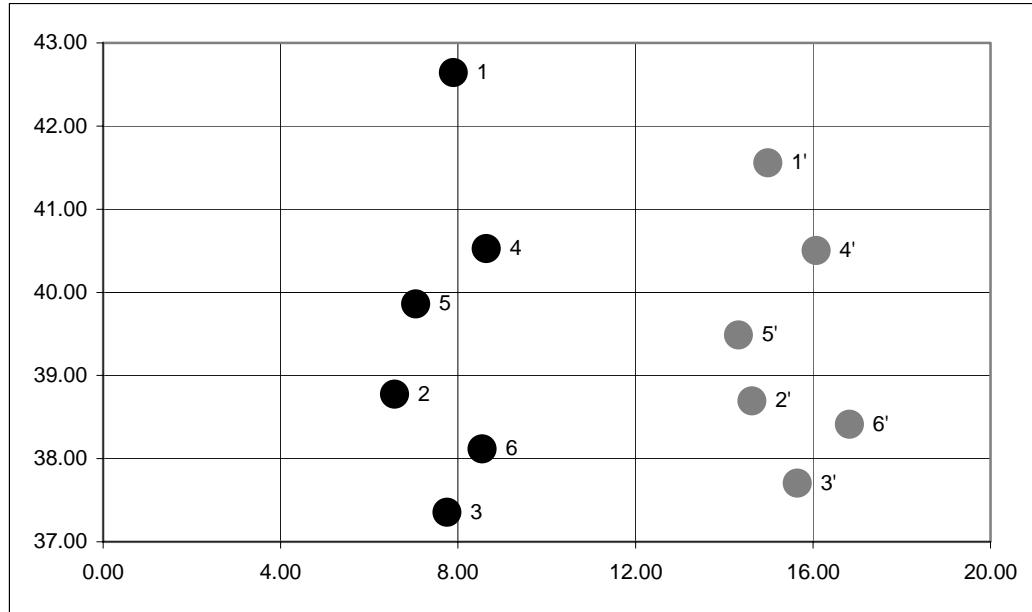
Figure 39.    Liquid atoms original and final configurations

Both the solid and liquid atoms are assumed to have an equal $x-direction$ force. The velocity profiles at different locations along the $x-axis$ in the $x-z$ plane are indicated in Figures 40 - 43. By observing these figures it can be concluded that due to the effect of the particles' (i.e., solid atoms') drag at the center of the computational domain, the solid atoms have a great effect on the velocity profile. This effect is associated with a significant reduction in the $x-direction$ velocity in all profiles; these results are expected, according to our results and discussions of the particles injection obtained by CFD solver. The similar effect of the injection can be found in Appendix A.
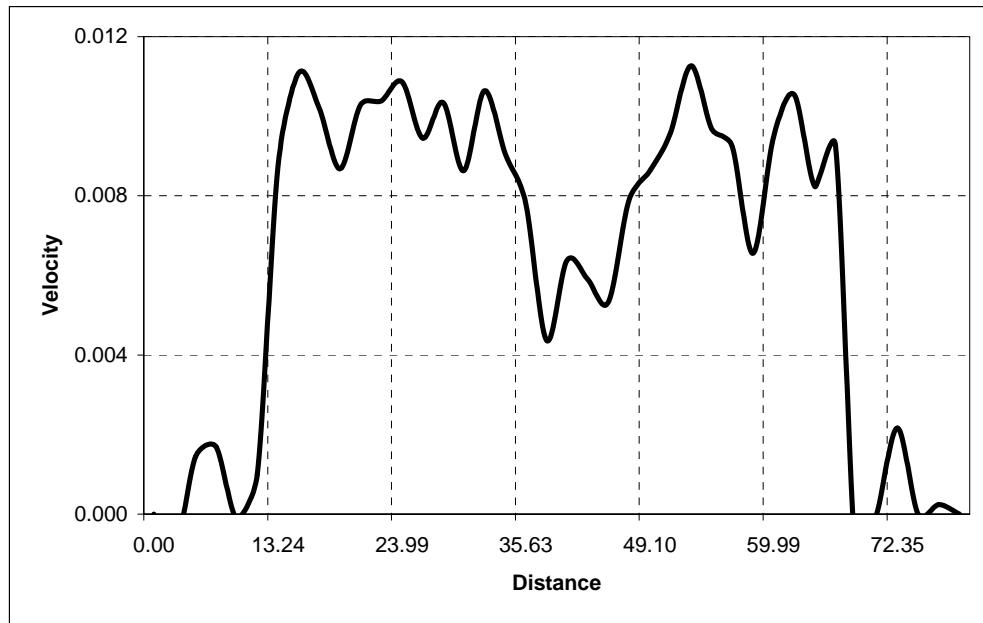
Figure 40.    Particles-liquid velocity profile at $x = 4$
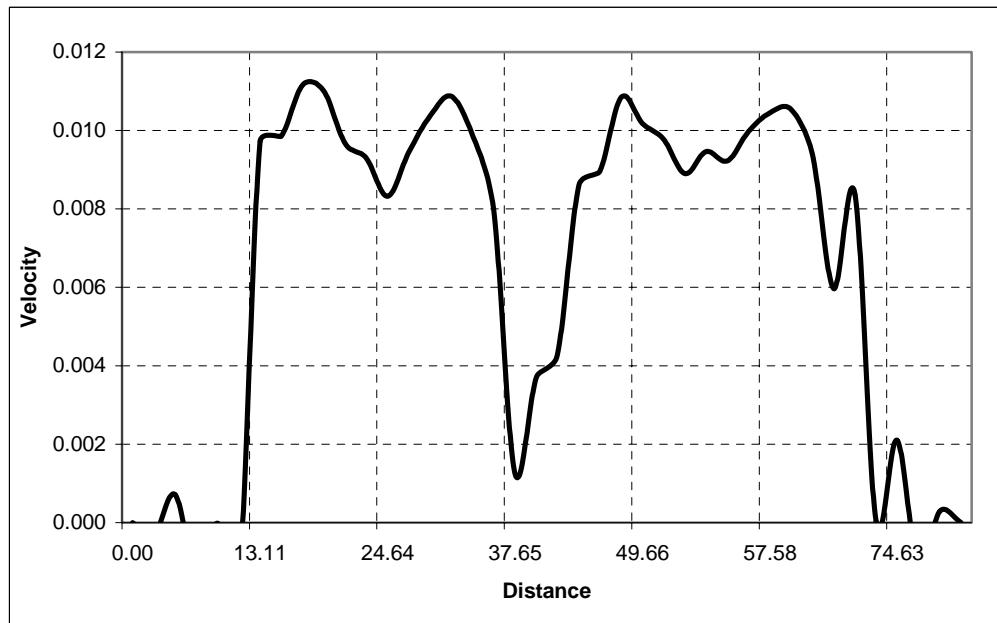


Figure 41.    Particles-liquid velocity profile at $x = 20$
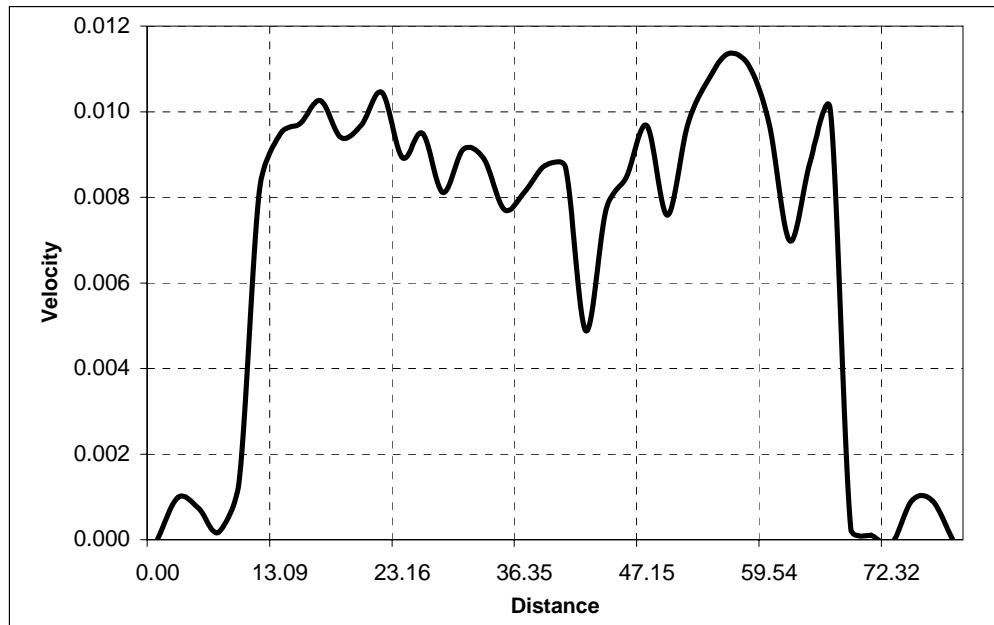
Figure 42.      Particles-liquid velocity profile at $x = 32$
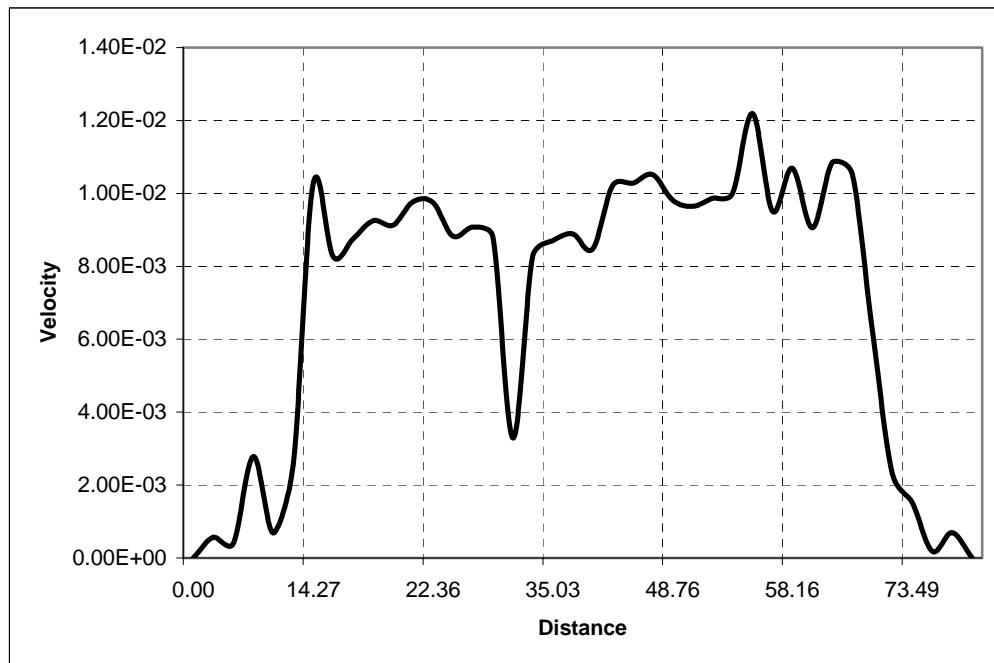


Figure 43.      Particles-liquid velocity profile at $x = 37$

## 2.    Three Vertical Solid Particles-Fluid Interaction

Three vertical particles were used at different locations as shown in Figures 44 in which the three particles (each particle has 6 atoms) have the same $x-coordinate$ value. The results are shown in Figures 45-48. Figure 45 shows that the particles drag force has a great effect on the velocity profile at $x = 4$. As the flow developed at $x = 20$ the particles effect will reduce. In addition, it can be noticed that the particle located at the center has the greatest effect on the flow as expected.
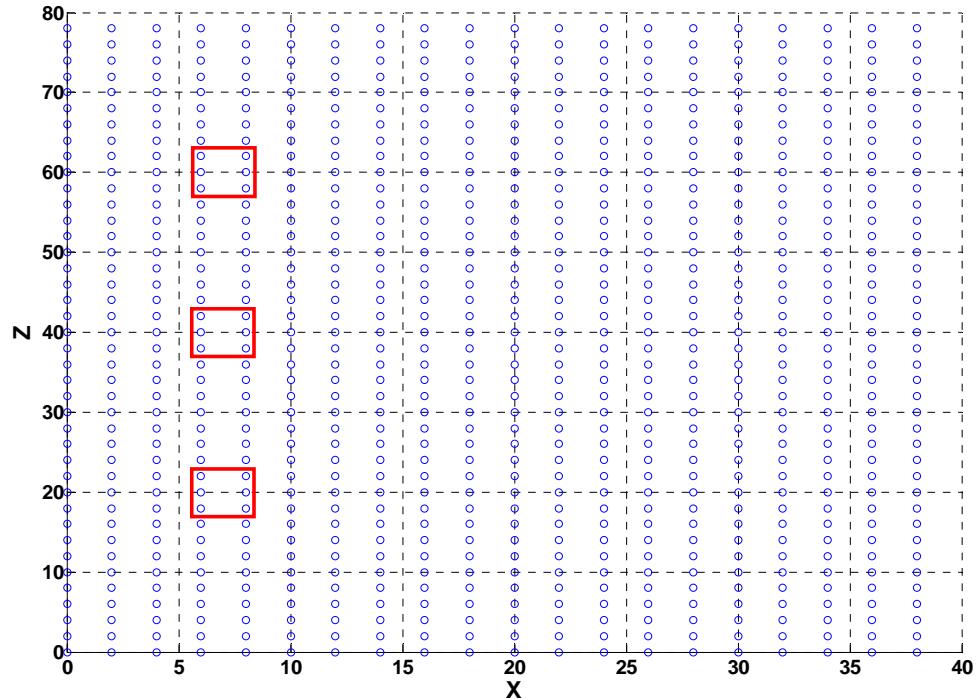


Figure 44.    3-vertical solid particles locations
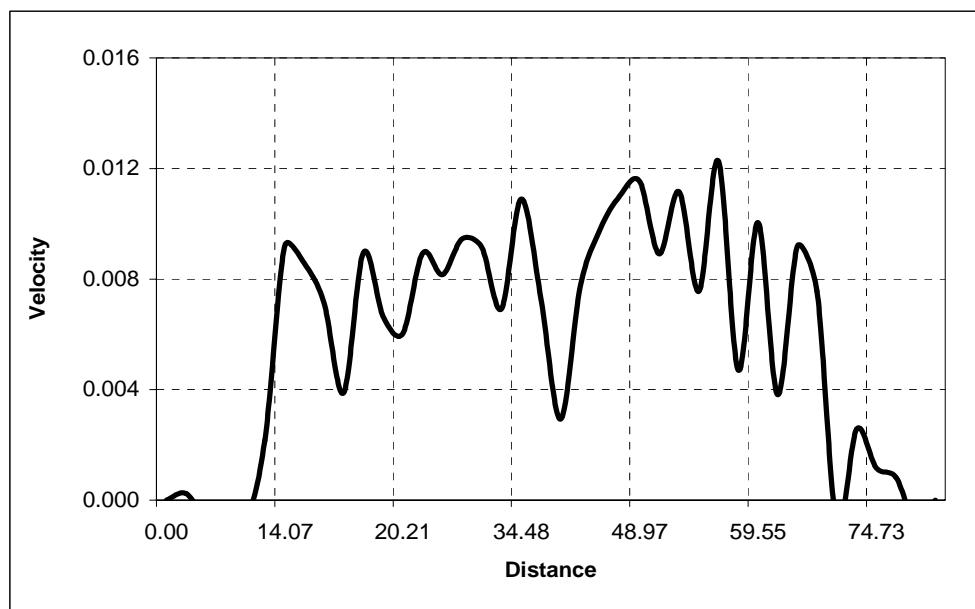
Figure 45.      3-vertical solid-fluid interaction at $x = 4$
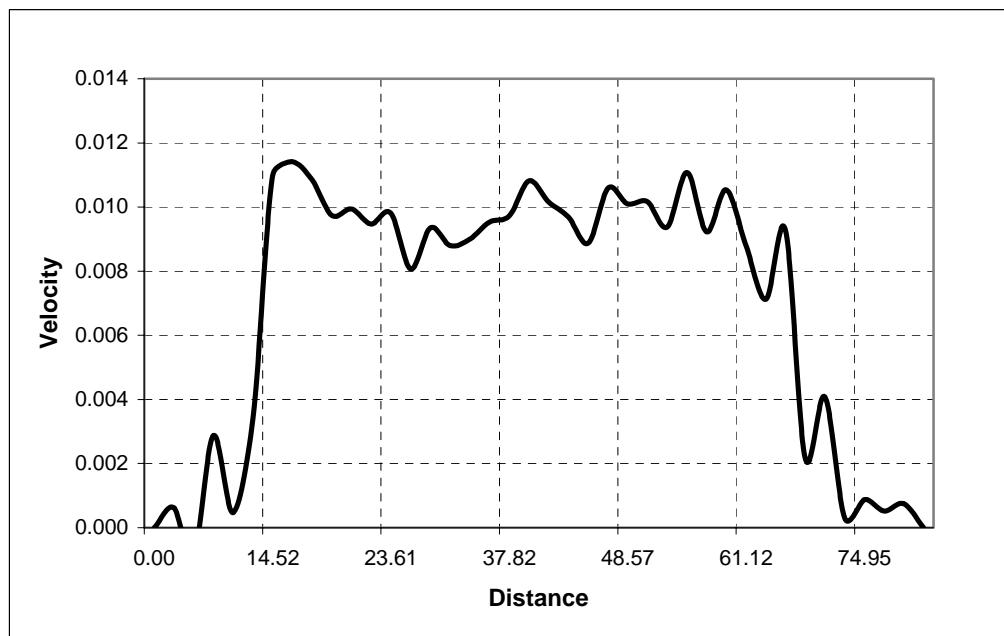


Figure 46.      3-vertical solid-fluid interaction at $x = 20$
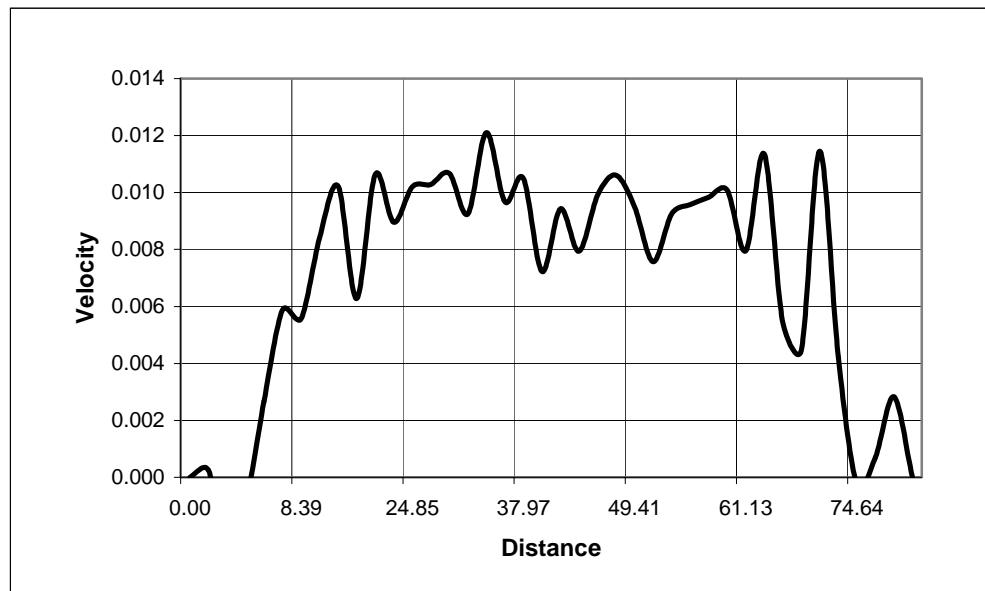
Figure 47.    3-vertical solid-fluid interaction at $x = 32$
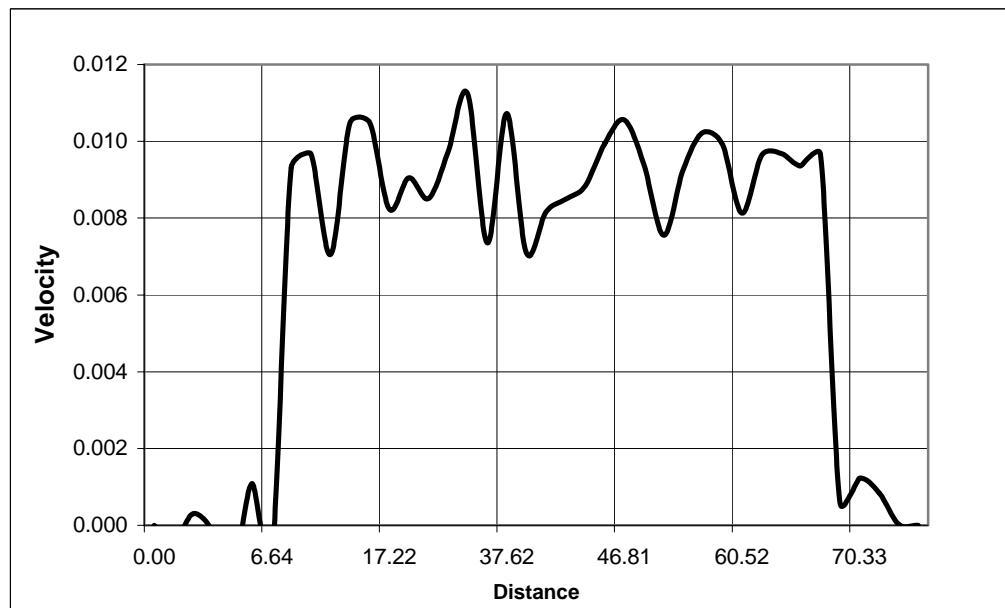


Figure 48.    3-vertical solid-fluid interaction at $x = 37$

### 3. Two Vertical Solid Particles-Fluid Interaction

In this case, two vertical solid particles, each with 18 atoms, were used as shown in Figure 49. Figures 50-53 indicate that the large particles have more effect on the velocity profile compared to the smaller one. This is because the intermolecular force between the solid and liquid atoms will increase. In fact using large particles must be avoided due to the tremendous effect on the working fluid behavior. Furthermore using large particles can be resulted in clogging the domain as explained before in Chapter IV.
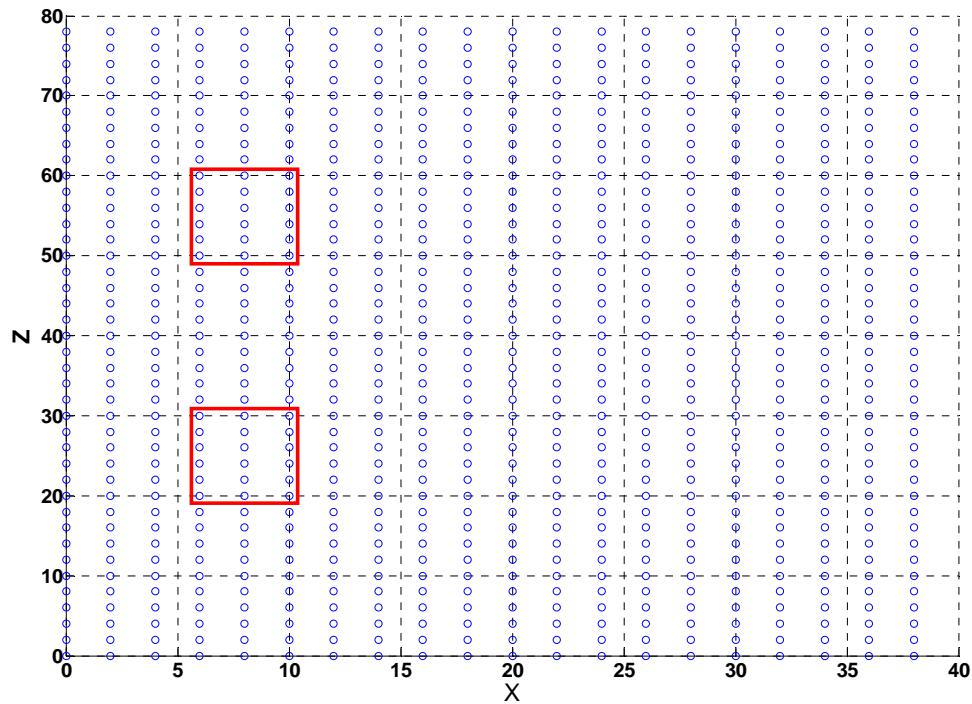


Figure 49.    3-vertical solid particles locations
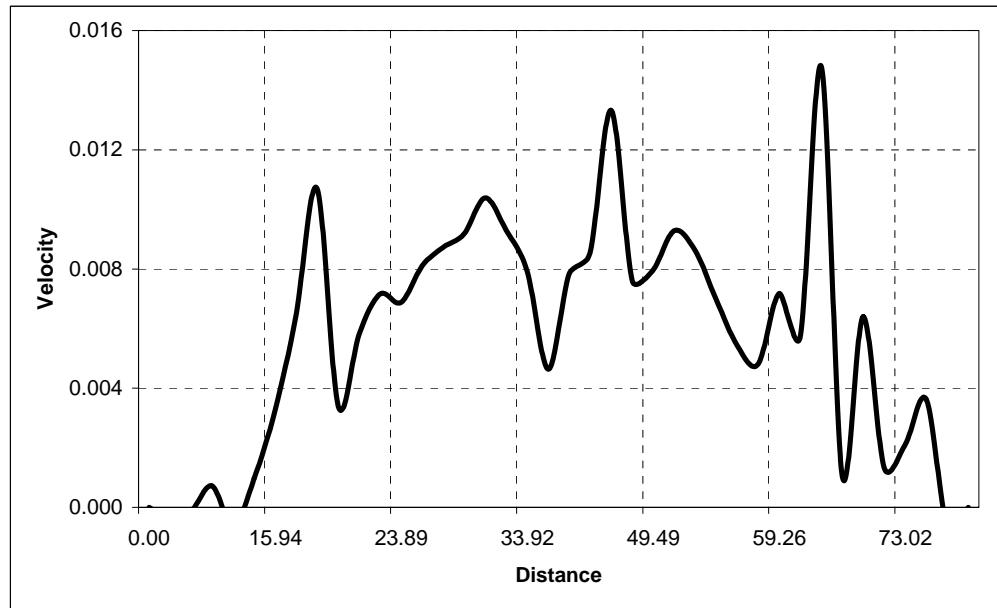
Figure 50.　2-vertical solid-fluid interaction at $x = 4$
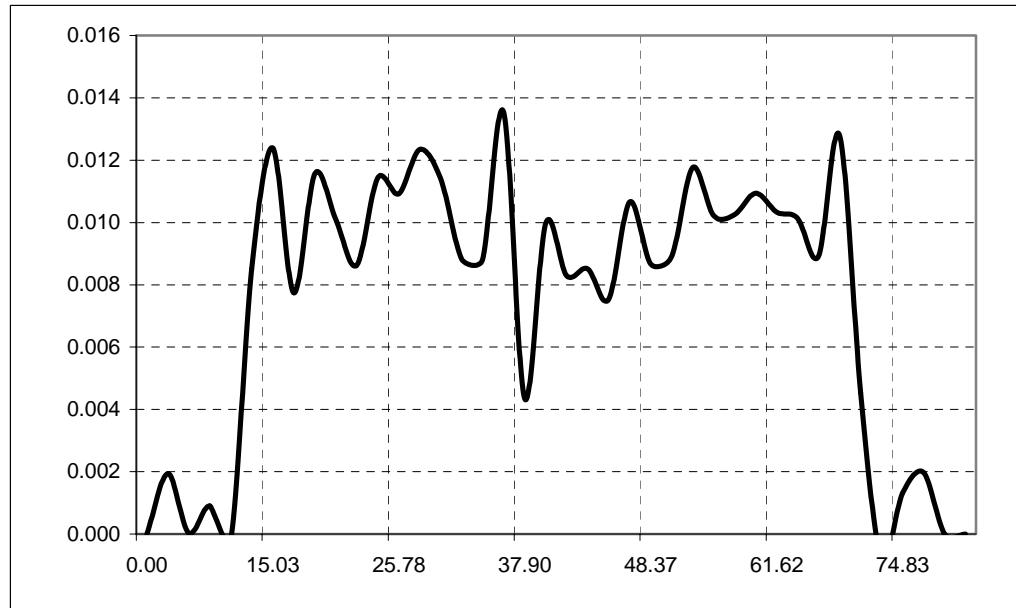


Figure 51.　2-vertical solid-fluid interaction at $x = 20$
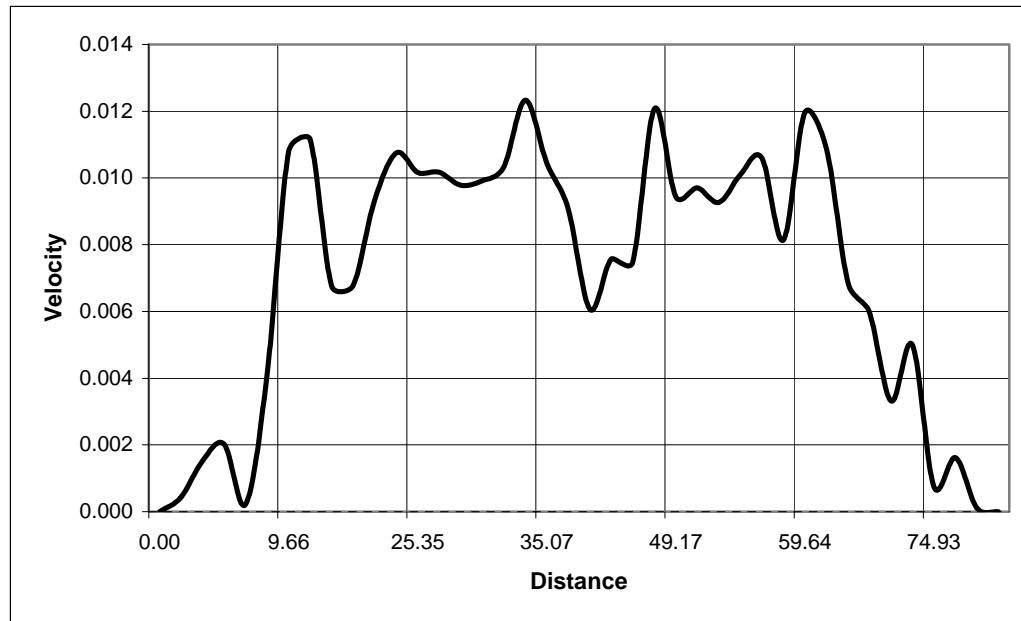
Figure 52.        2-vertical solid-fluid interaction at $x = 32$
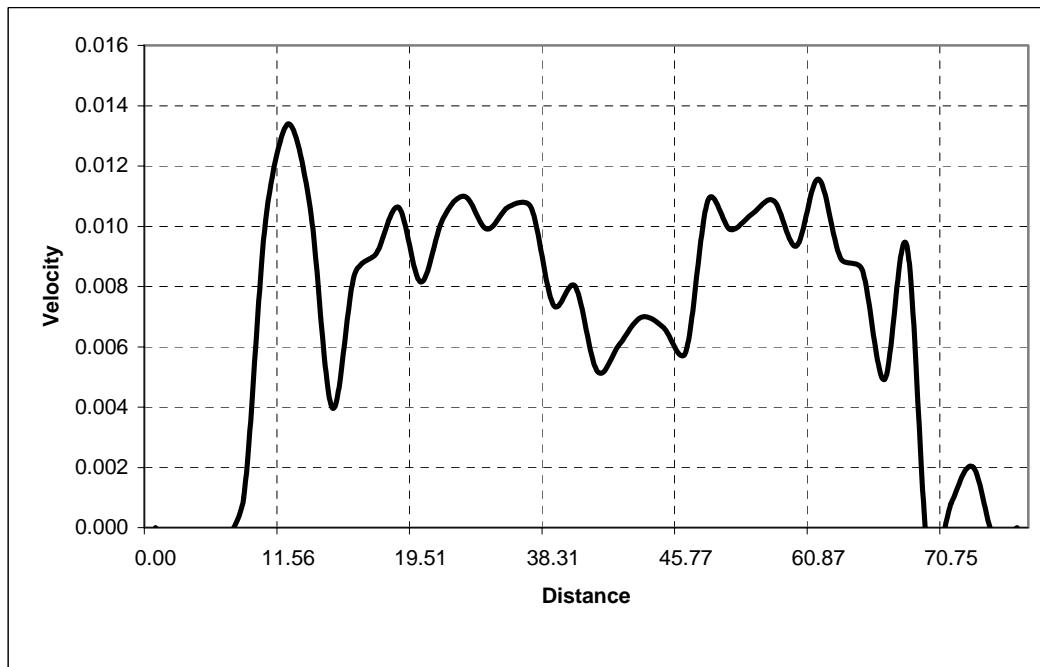


Figure 53.        2-vertical solid-fluid interaction at $x = 32$

## C. RANDOM PARTICLES-FLUID INTERACTION

In this case the particles are represented as a group of solid atoms. These particles are assigned at random locations throughout the domain, as indicated in Figure 44 below. The all atoms except for the boundary solid atoms have a $x-direction$ force $f_{xf} = 0.1$.
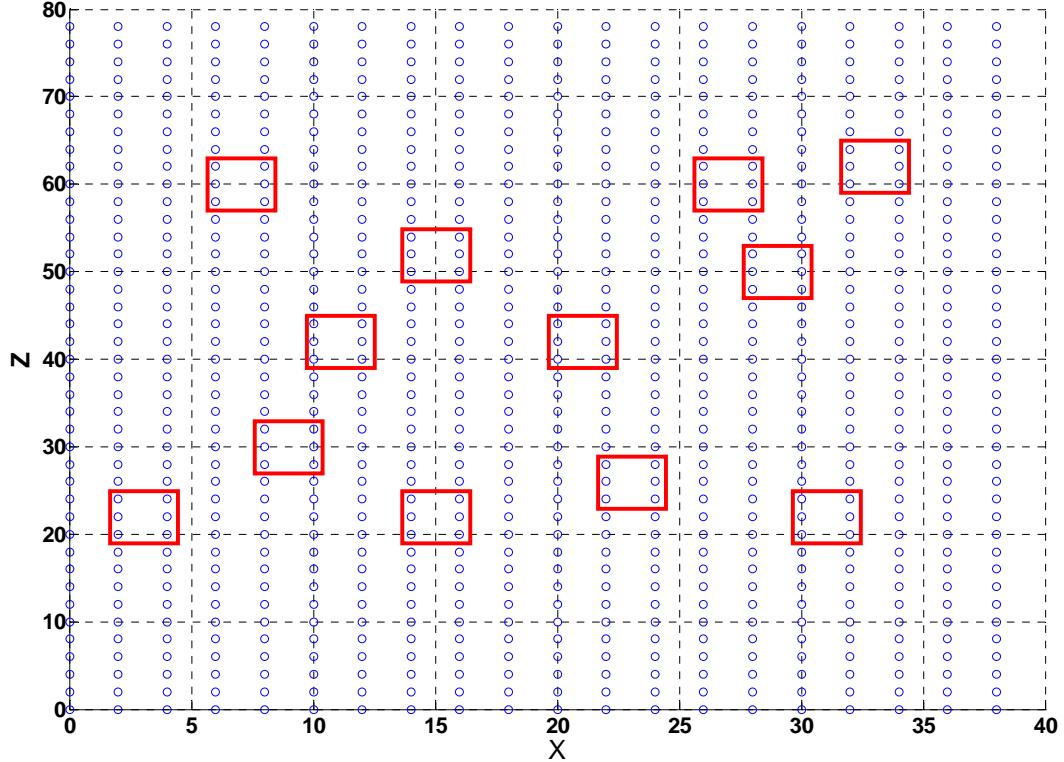


Figure 54.     Solid-liquid atoms configurations

As stated in the beginning of this chapter, the obtained results have a significant amount of atomic motion. The concept of particles' drag forces still exist, as indicated in Figure 45. It can be noticed that the particles atoms located between $x = 30$ and $x = 35$ have the greatest effect on the velocity profile obtained at $x = 37$. Furthermore, as expected, the particles that are closer to the profile have more effect on its shape.

60
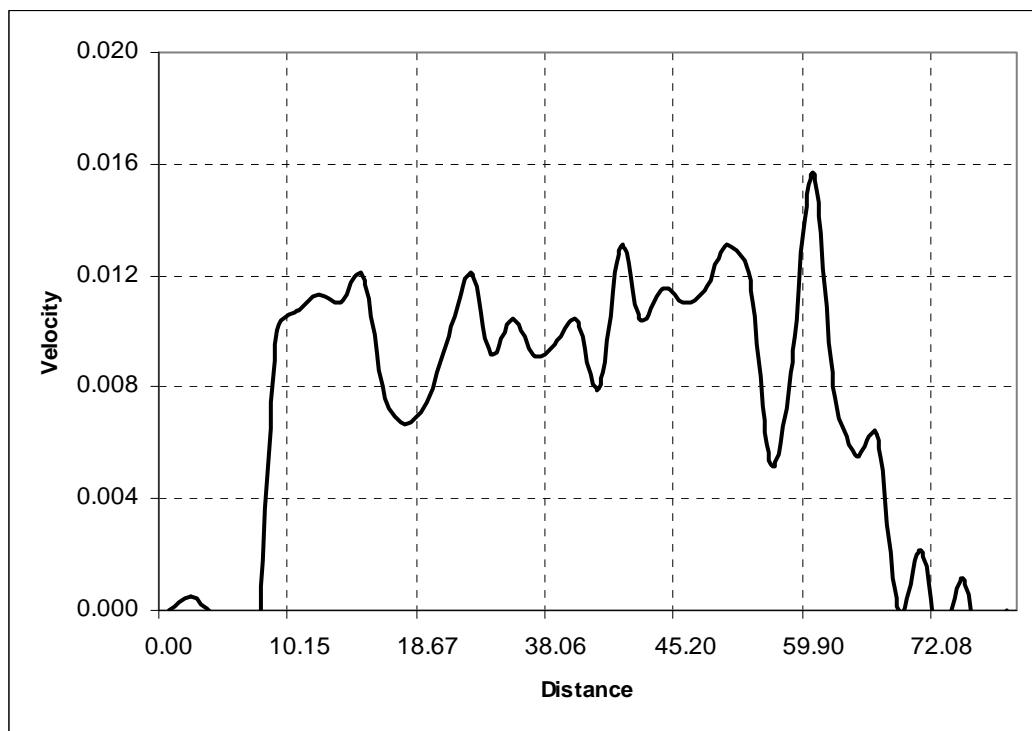
Figure 55.    Random particles-liquid interaction velocity profile at
$x = 37$

THIS PAGE INTENTIONALLY LEFT BLANK

# VI.   CONCLUSIONS AND RECOMMENDATIONS


Solid particles-liquid interaction was studied in two different levels: continuum level and atomic level. At the continuum level, the effect of micro-scale particles injection was examined on the enhancement of heat transfer, fluid velocity profile, and the pressure to the boundary walls.  The study showed that the effect of particles was greater for the laminar flow but negligible for the turbulent flow.  For the laminar flow, the location of the particle injection and their mass rate affected significantly the flow velocity profiles as well as the pressure on the boundary walls.  The pressure is critical for structural integrity of the wall as well as flow-induced vibration. As far as the enhancement of heat transfer was concerned, there was a marginal benefit. However, this result was for a very small volume of particles. If the particle volume were increased, the heat transfer effect would be more significant.

The atomic level study using molecular dynamics agreed qualitatively with the continuum result in terms of the fluid atomic velocity affected by solid atoms. According to this study and analysis, it was found that the best particles injection location was the center of the inlet domain. This location had a good heat transfer potential enhancement as well as avoided any kind of significant pipe/tube vibration that could occur due to the variation in the upper and lower wall pressures.  Other injection locations resulted significant effect on the pressure variation inside the domain, that can result in tube/pipe vibration.

By using the CFD ACE+ Multi-physics commercial program to simulate a macro particles injection through a continuous media of fluid flow under different injections conditions as well as performing the molecular dynamics simulation program to simulate particles-liquid interaction in a nano-scale model using a system of atoms, the following recommendations can be made:

Current CFD requires additional improvement to simulate the type of problems involving nano and macro scales. Current limitations in these programs, such as the

difficulty of simulating more than one injector, do not address situations important for particle-fluid interaction applications.

As demonstrated from our calculations, particles injection is a very useful technique to improve the heat transfer potential. Therefore this method of potential enhancement should be further investigated.

Although the molecular dynamics simulation is a very accurate program in obtaining accurate physical properties, it requires much effort to obtain the correct configuration for the system of molecules of interest. Furthermore it requires a significant amount of time and a powerful set of computer systems. A more efficient computational method is desirable.

Molecular dynamics is widely used in many chemical and physical and combustion applications. However, it is rarely found as an important and accurate simulation technique in solid-liquid applications, and therefore this field is wide open for additional research.

# APPENDIX A. LAMINAR FLOW SIMULATION SERIES

**1.    Injector located at** $\left(0, 4\times10^{-4}, 0\right)$
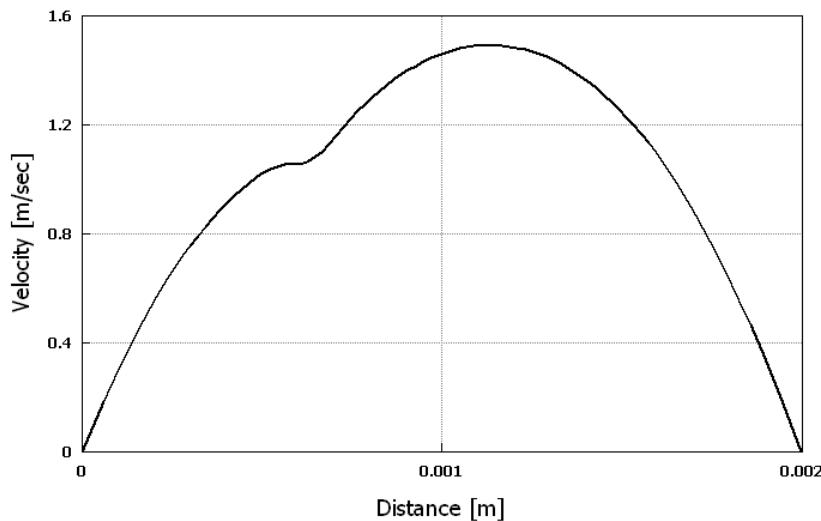


Figure A1. Velocity profile at $x = 0.01$
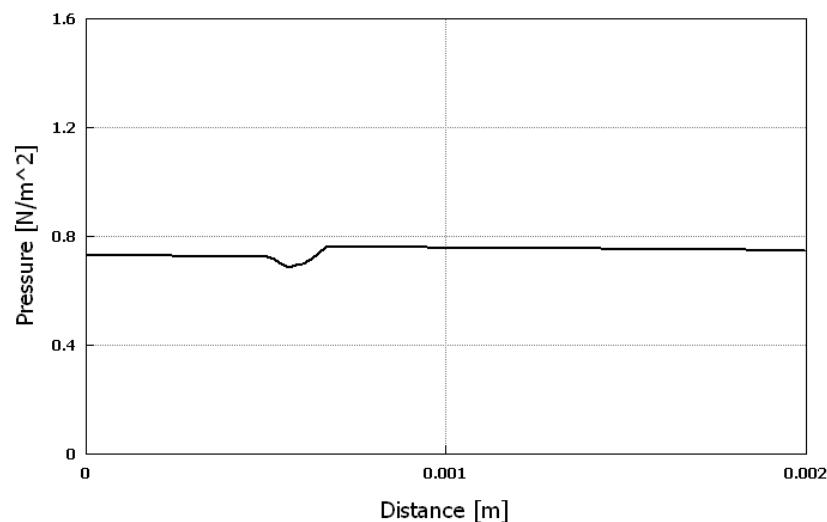


Figure A2. Pressure distribution along $y - axis$ at $x = 0.01$
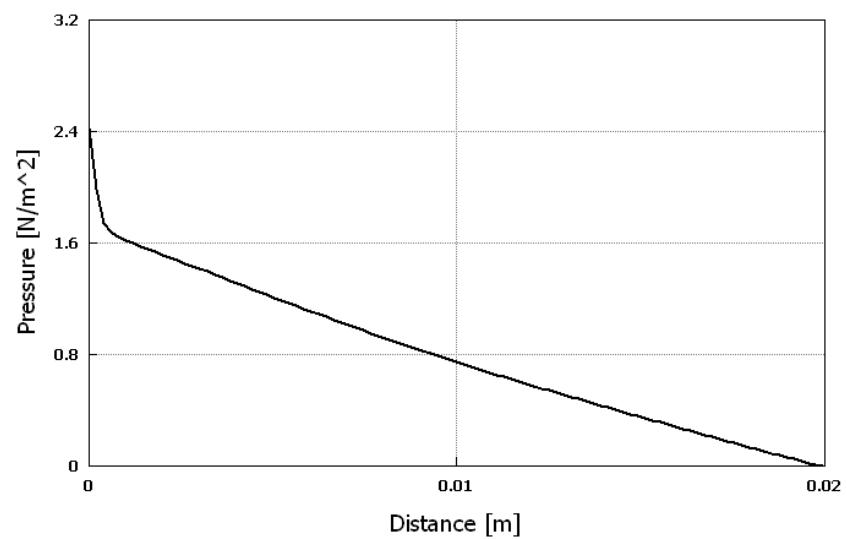
Figure A3. Upper wall pressure distribution along $x-axis$
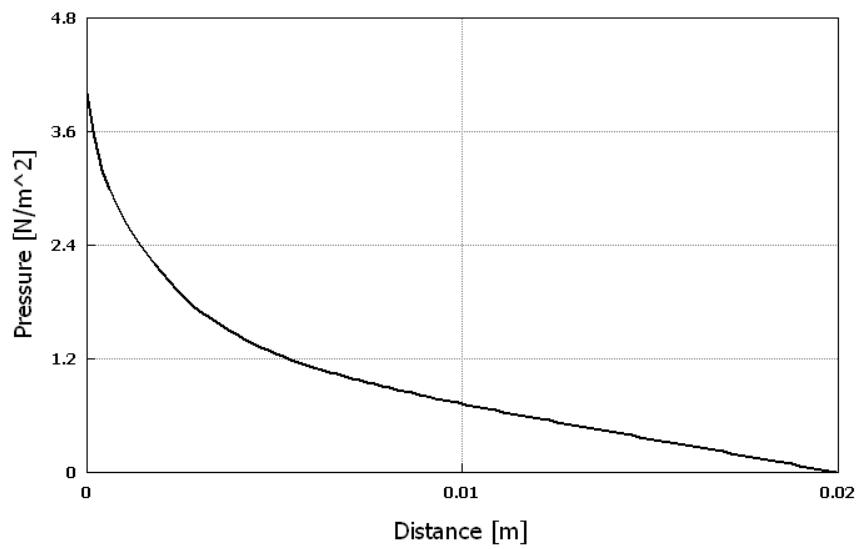


Figure A4. Lower wall pressure distribution along $x-axis$

## 2. Injector located at $\left(0, 6\times10^{-4}, 0\right)$
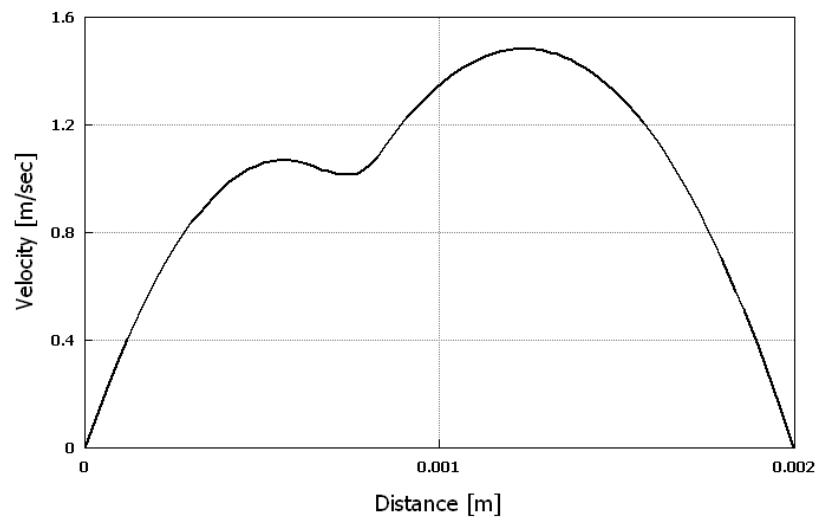


Figure A5. Velocity profile at $x = 0.01$
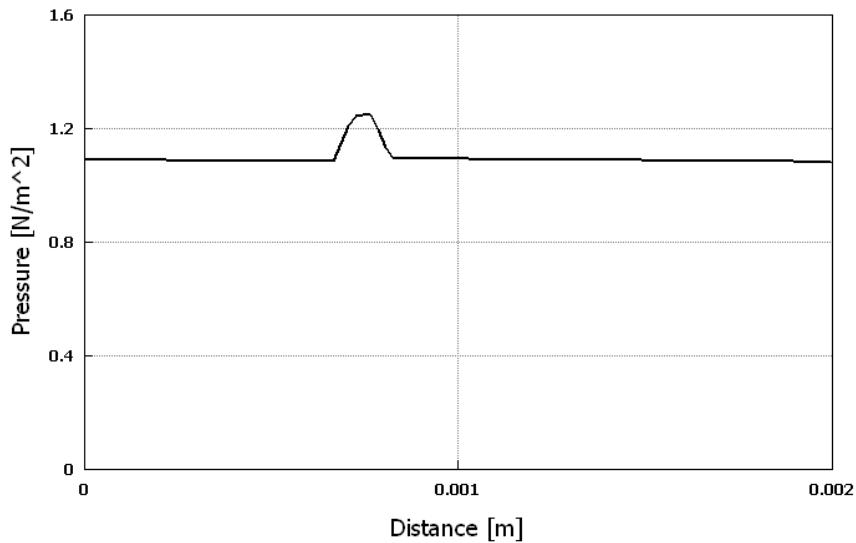


Figure A6. Pressure distribution along $y - axis$ at $x = 0.01$
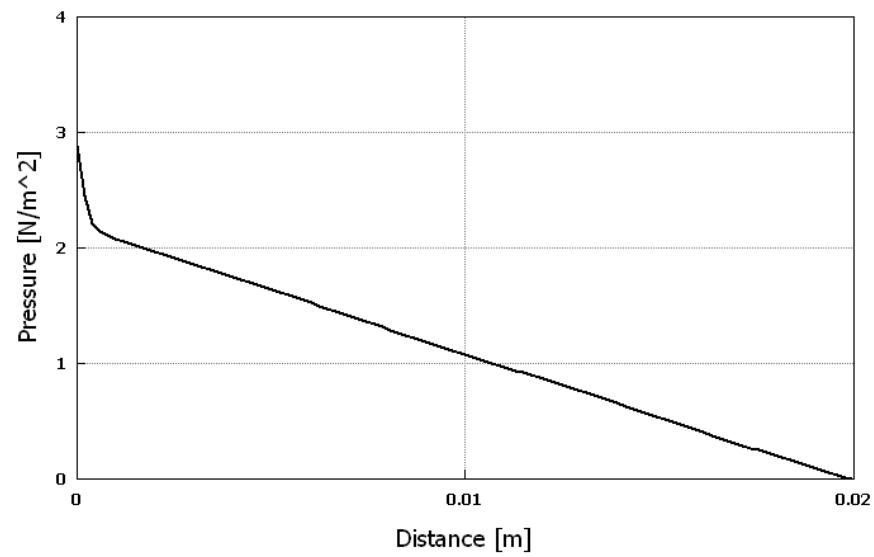
Figure A7. Upper wall pressure distribution along $x - axis$
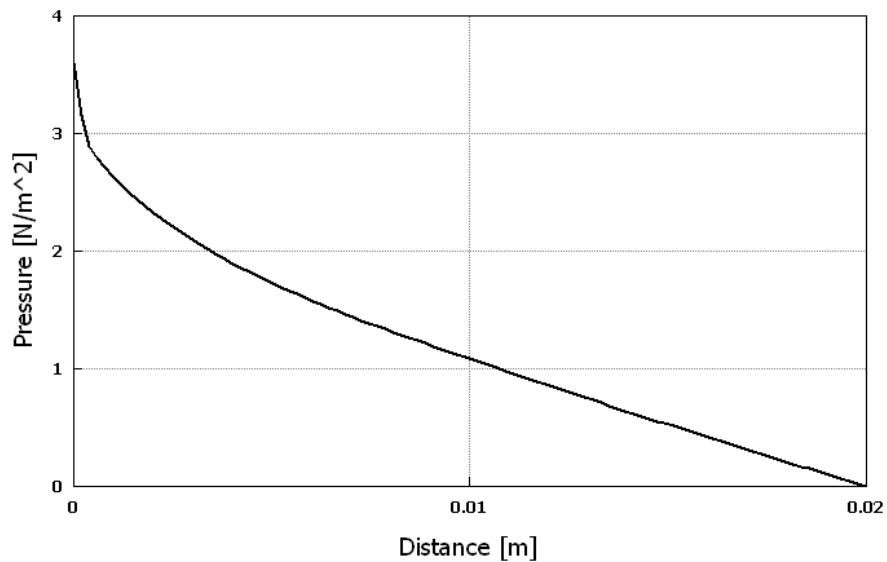


Figure A8. Lower wall pressure distribution along $x - axis$

## 3. Injector located at $(0, 1 \times 10^{-3}, 0)$
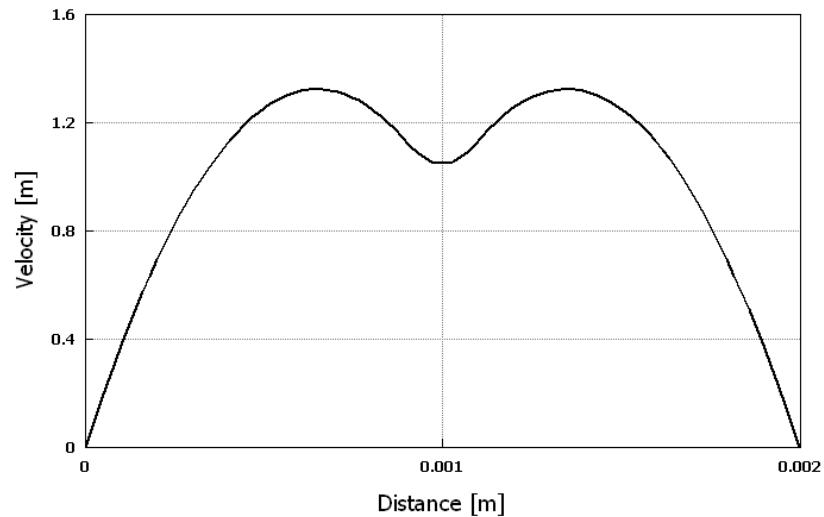


Figure A9. Velocity profile at $x = 0.01$
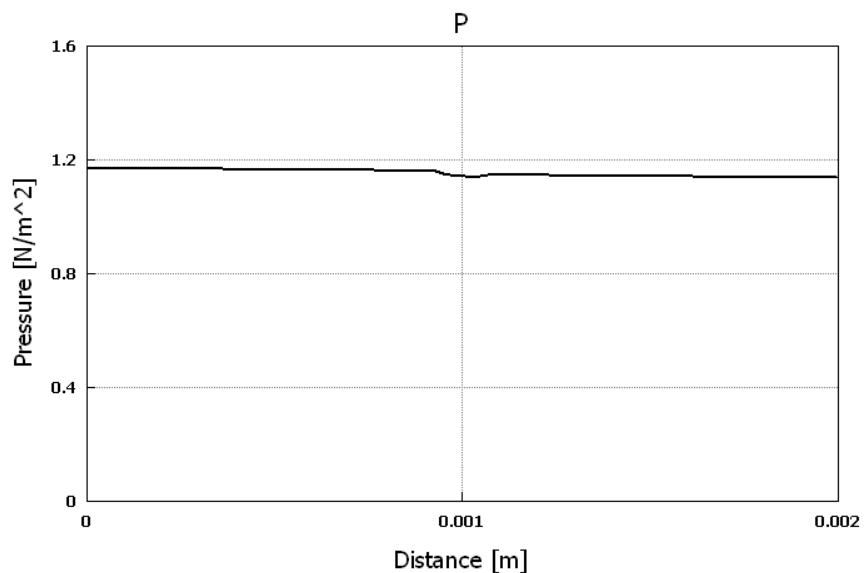


Figure A10. Pressure distribution along $y - axis$ at $x = 0.01$

69
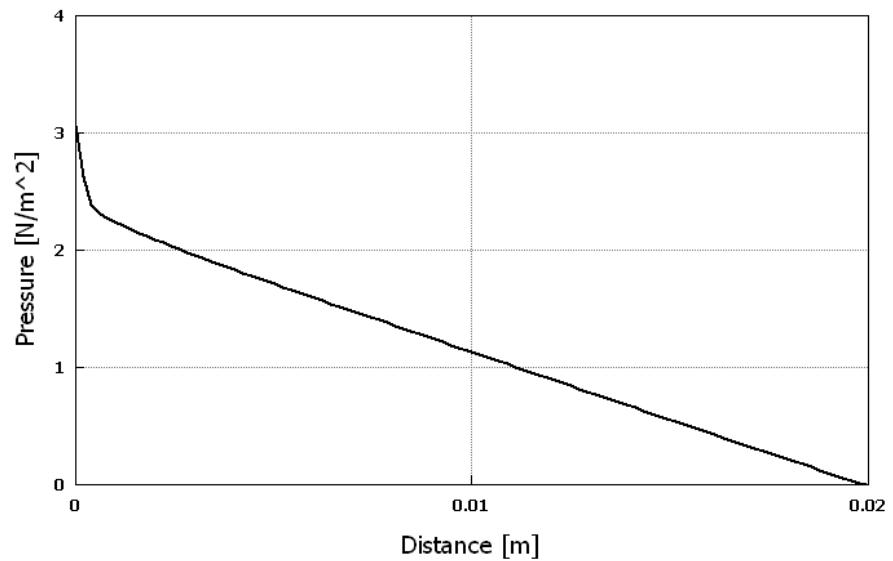
Figure A11. Upper wall pressure distribution along $x-axis$
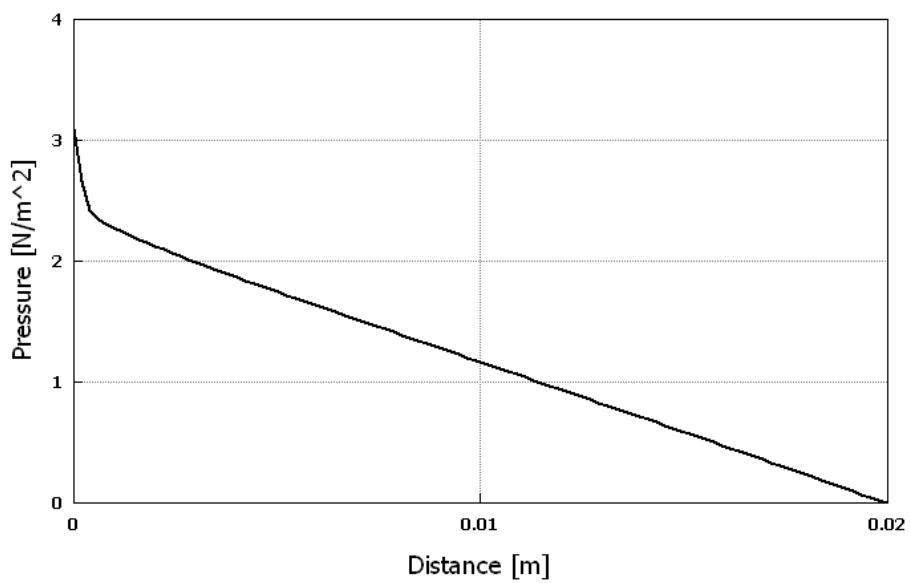


Figure A12. Lower wall pressure distribution along $x-axis$

70

# APPENDIX B.     TURBULENT FLOW SIMULATION SERIES

**1.      Injector located at** $\left(0, 4 \times 10^{-4}, 0\right)$
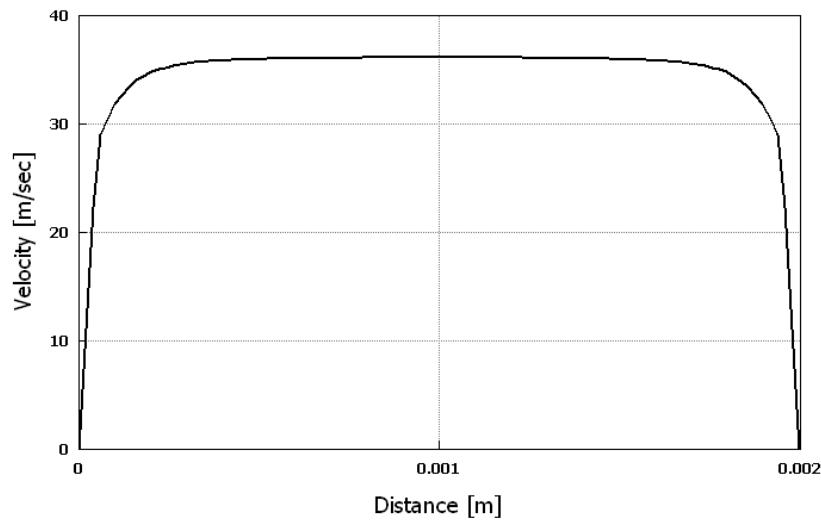


Figure B1. Velocity profile at $x = 0.01$
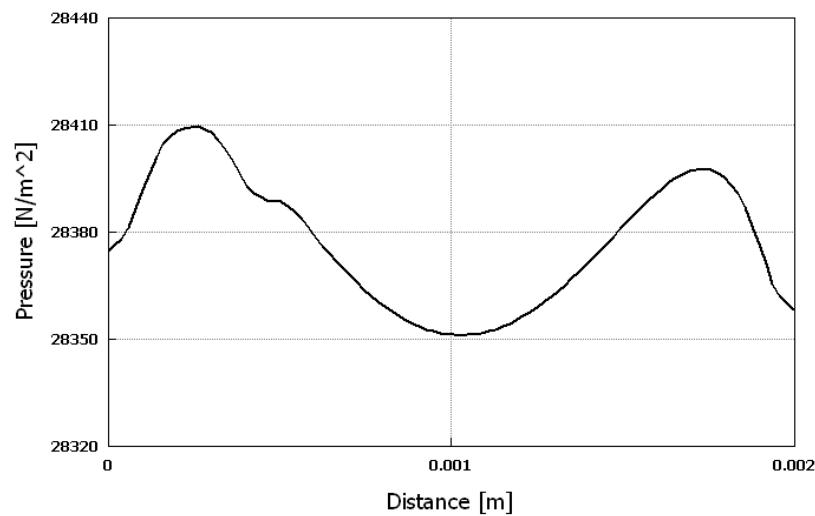


Figure B2. Pressure distribution along $y - axis$ at $x = 0.01$
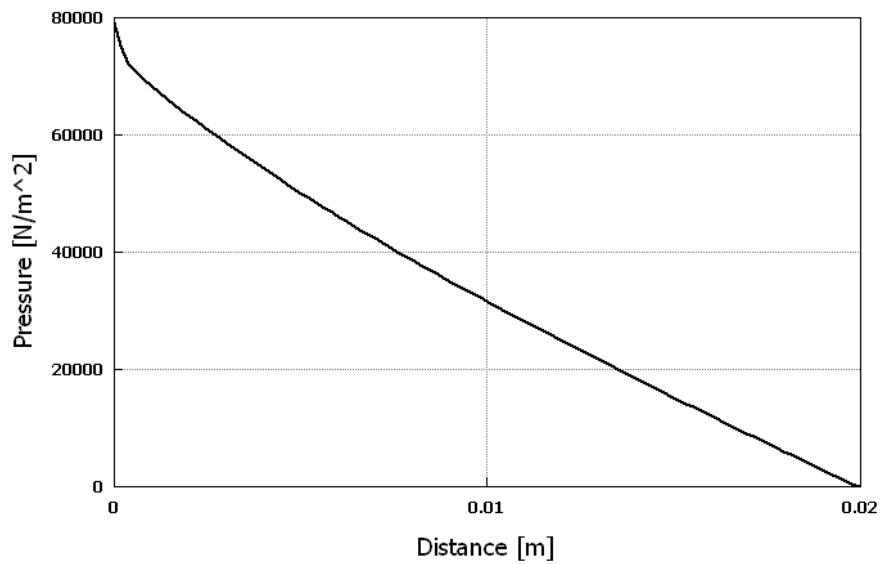
Figure B3. Upper wall pressure distribution along $x-axis$
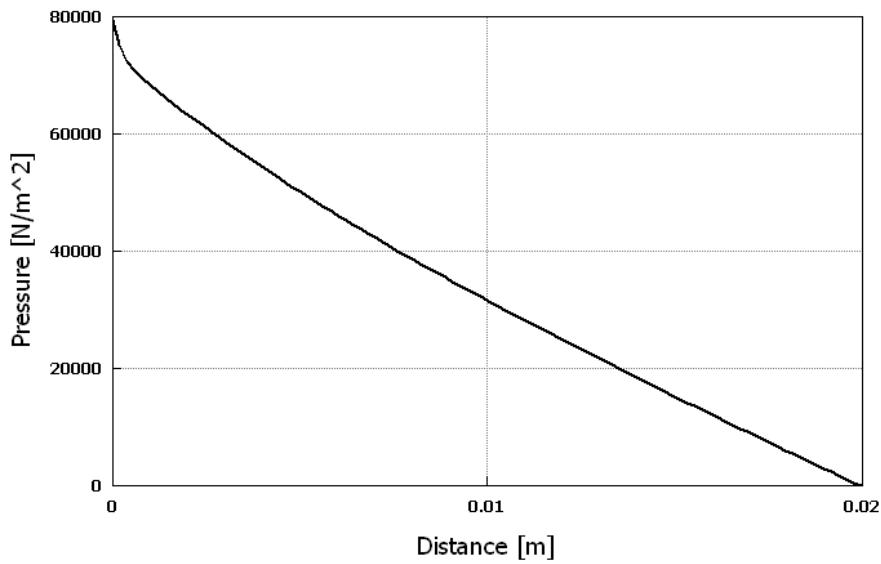


Figure B4. Lower wall pressure distribution along $x-axis$

72

**2.    Injector located at** $\left(0, 6 \times 10^{-4}, 0\right)$



Figure B5. Velocity profile at $x = 0.01$
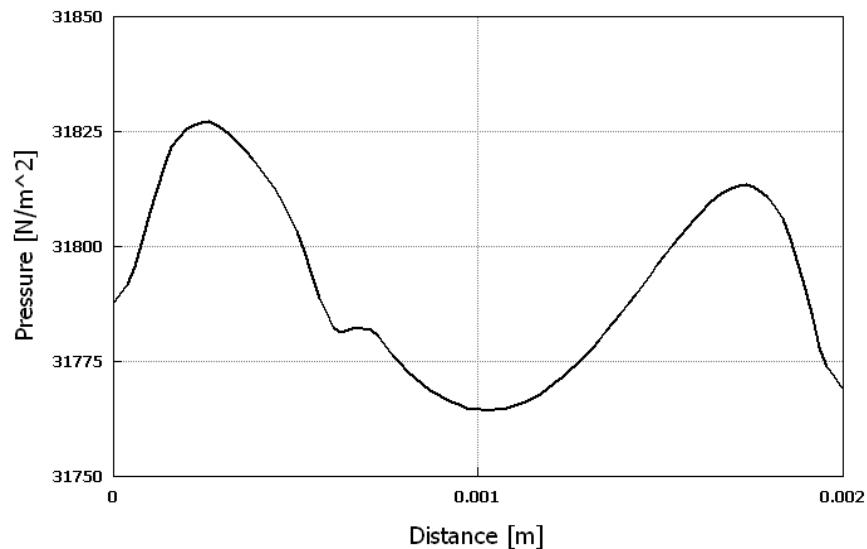


Figure B6. Pressure distribution along $y - axis$ at $x = 0.01$

73
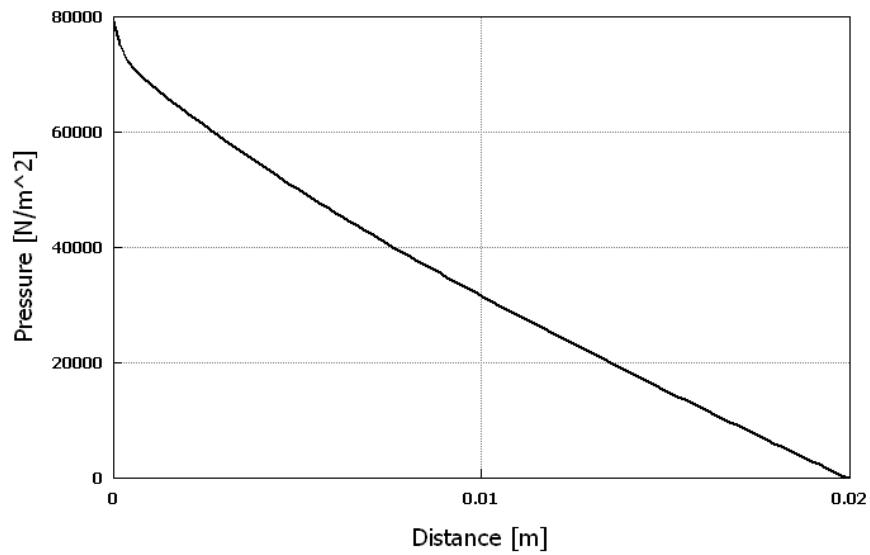
Figure B7. Upper wall pressure distribution along $x-axis$
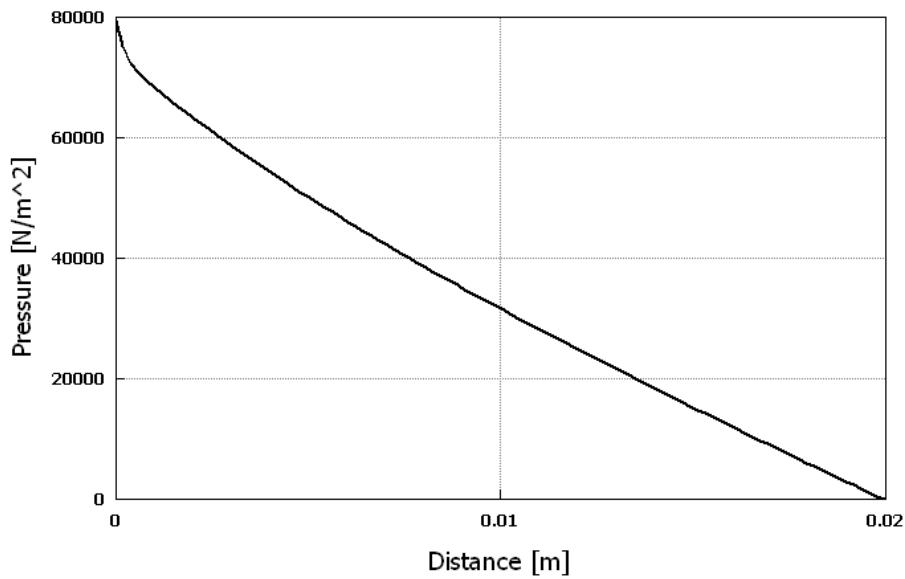


Figure B8. Lower wall pressure distribution along $x-axis$

**3.** **Injector located at** $\left(0,1\times10^{-3},0\right)$
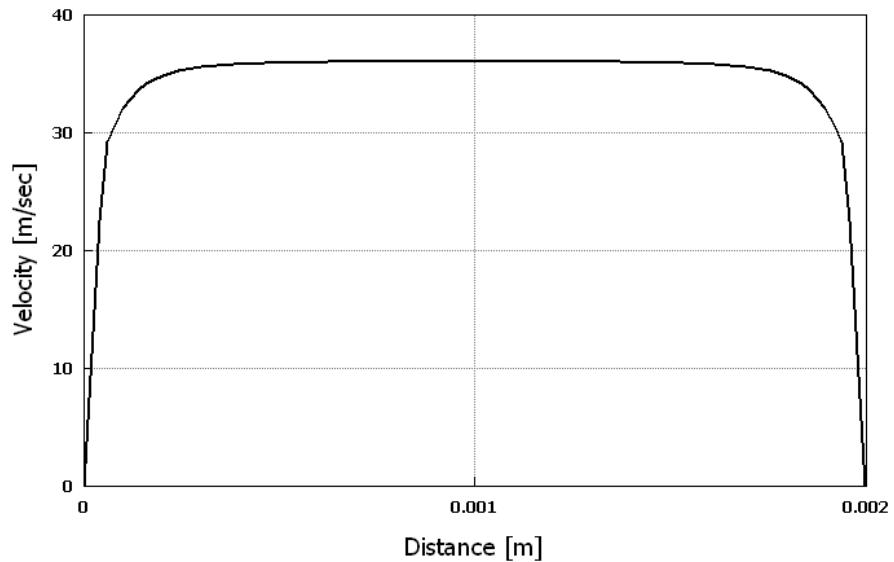


Figure B9. Velocity profile at $x = 0.01$
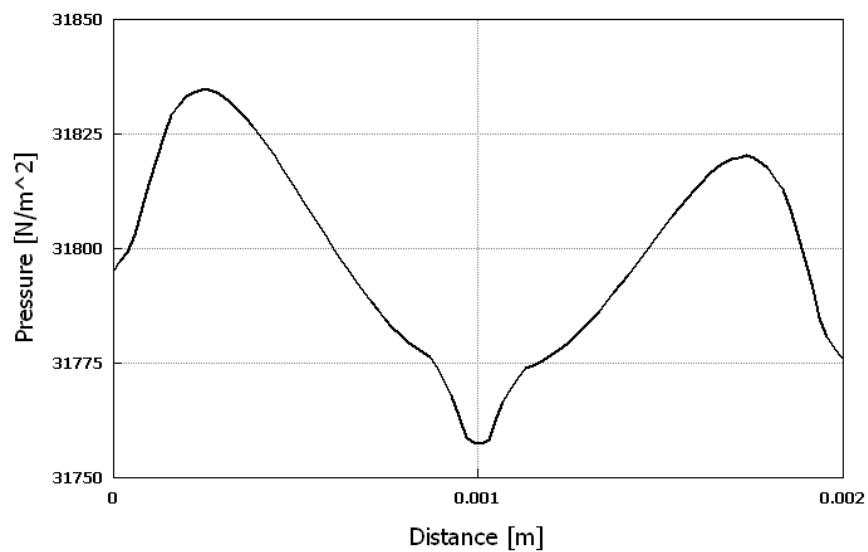


Figure B10. Pressure distribution along $y-axis$ at $x = 0.01$
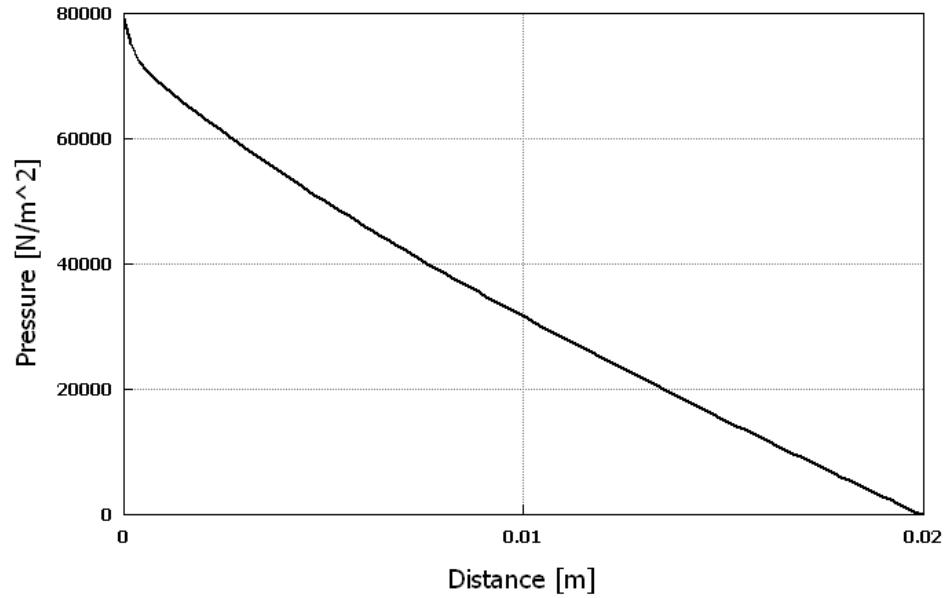
Figure B11. Upper wall pressure distribution along $x - axis$
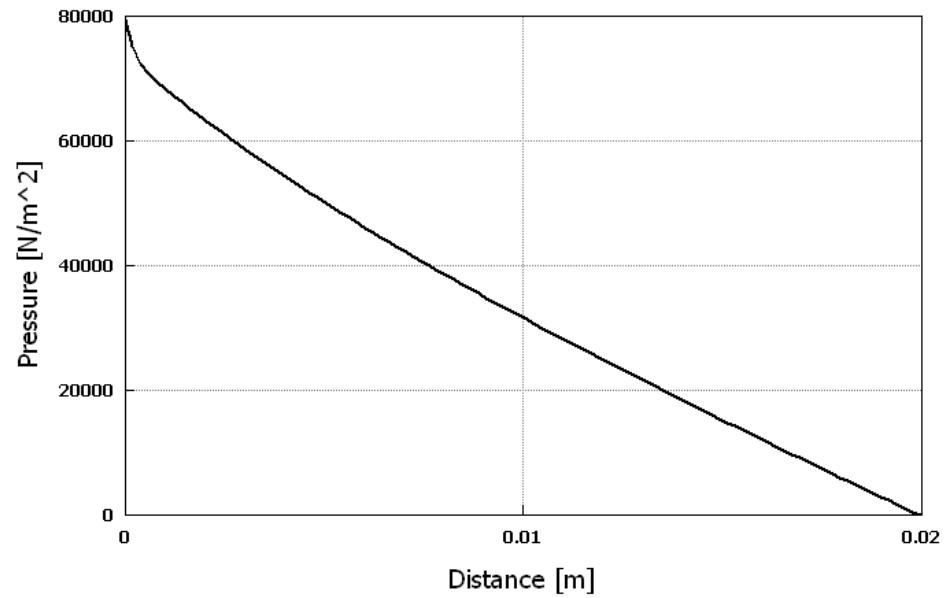


Figure B12. Lower wall pressure distribution along LIST OF REFERENCES

# LIST OF REFERENCES

[1]     CFD-ACE+ V2004 Modules Manual,ESI CFD Inc.,2004.

[2]     Q. Zhang, R. Lec, and K. Pourrezai, "The study of an interaction of solid particles with various surfaces using TSM sensors," IEEE,2003.

[3]     H. Gan, J. J. Feng, ad H. H. Hu, "Simulation of the sedimentation of melting solid particles, "International Journal of Multiphase Flow, vol. 19, pp. 751-769, February 2003.

[4]     E. Onate, S. R. Idelsohn, M. A. Veligueta, and R. Rossi, "Advances in the particle finite element method for fluid-structure interaction problems," International Center for Numerical Methods in Engineering (CIMNE), Spain.

[5]     Z. OC, and T. RL, "The finite element method for fluid dynamics, " Elsevier, 2006.

[6]     O. C. Nwobi, L. N. Long, and M. M. Micci, "Molecular dynamics studies of thermophysical properties of supercritical ethylene," American Institute of Aerodynamics and Astronautically, 1998.

[7]     M.P. Allen, and D.J. Tildesley, "Computer simulation of liquids,"Clarendon Press, Oxford, 1$^{st}$ edition, 1987.

[8]     O. Genevaux, A. Habibi, J. M. Dischler, "Simulating fluid-solid interaction,"LSIIT UMR CNRS-ULP 7005, France.

[9]     C. Yunfei, L. Deyu, Y. Juekuan, W. Yonghua, L. R. Jennifer, and M. Arun, " Molecular dynamics study of the lattice thermal conductivity of Kr/Ar supperlattice nanowires," ELSEVIER, 2004.

[10]    L, Ju, L. Dongyi, and Y. Sidney, " Coupling continuum to molecular-synamics simulation: reflecting particle method and the field estimator," Physical Review E., vol. 57, June 1998.

[11]    F. M. White, Fluid Mechanics, fifth edition. New York: McGraw-Hill Education, 2003.

[12]    O. C. Nwobi, L. N. Long, and M. M. Micci, "Molecular dynamics studies of transport  properties of supercritical fluids," American Institute of Aerodynamics, January 1997.

[13]    B. J. Garrison," Molecular dynamics simulation of surface chemical reaction," Chem. Soc. Review, 21, pp155-162, 1992.

[14]    D. C. Rapaport," Mocroscale hydrodynamics discrete-particle simulation of evolving flow pattern," Physical Review A, 38, pp. 3288-3299, 1997.

[15]    J. E. Lennard-Jones,"The determination of molecular fields. I. from the variation of the viscosity of a gas with temperature," Proc. Roy. Soc., 1924.

[16]    J. E. Lennard-Jones,"The determination of molecular fields. II. from the equation of  state of the," Proc. Roy. Soc., 1924.

[17]    J. M. Haile, Molecular dynamics simulation, Elementary methods. New York: John Wiley & Sons, 1997.d

[18]    Lennard-Jones fluid,

http://www.plmsc.psu.edu/~www/matsc597c-1997/simulations/Lecture3/ node1.html (13 Nov 07).

# INITIAL DISTRIBUTION LIST

1. Defense Technical Information Center
   Ft. Belvoir, Virginia

2. Dudley Knox Library
   Naval Postgraduate School
   Monterey, California

3. Young W. Kwon
   Professor
   Mechanical and Astronautical Engineering
   Naval Postgraduate School
   Monterey, California

4. Commander Royal Bahraini Naval Force
   Bahrain Defense Force
   Kingdom of Bahrain

5. Director of Military Training
   Bahrain Defense Force
   Kingdom of Bahrain

6. Jamal S. AlRowaijeh
   Engineering Officer
   Royal Bahraini Naval Force
   Bahrain Defense Force
   Kingdom of Bahrain